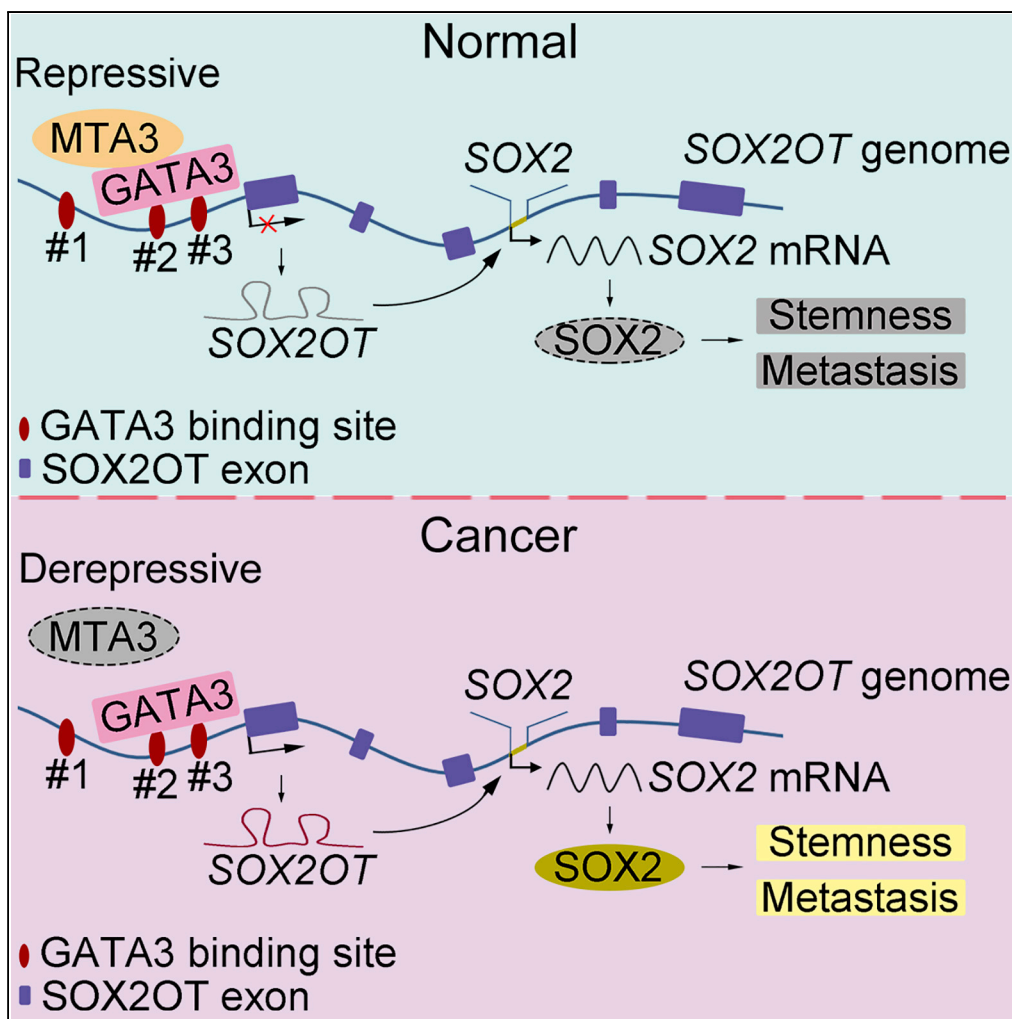**Article**

MTA3 Represses Cancer Stemness by Targeting the SOX2OT/SOX2 Axis

Liang Du, Lu Wang, Jinfeng Gan, ..., Robert P. Coppes, Dianzheng Zhang, Hao Zhang

zhoufuyou007@163.com (F.Z.)
haozhang@jnu.edu.cn (H.Z.)

HIGHLIGHTS

MTA3 is recruited by GATA3 to repress SOX2OT transcription

The MTA3/GATA3 complex dampens SOX2 signaling by inhibiting SOX2OT transcription

MTA3 can repress both cancer stemness and metastasis of squamous esophageal cancer

Low MTA3 and high SOX2 expression predicts poor prognosis in esophageal cancer

Article

MTA3 Represses Cancer Stemness by Targeting the SOX2OT/SOX2 Axis

Liang Du,[1,2,3,4,14] Lu Wang,[1,2,14] Jinfeng Gan,[2,3,14] Zhimeng Yao,[2,3] Wan Lin,[3] Junkuo Li,[5,6] Yi Guo,[7] Yuping Chen,[8] Fuyou Zhou,[5,6,*] Sai-Ching Jim Yeung,[9,10] Robert P. Coppes,[4] Dianzheng Zhang,[11,12] and Hao Zhang[1,2,13,15,*]

SUMMARY

Cancer cell stemness (CCS) plays critical roles in both malignancy maintenance and metastasis, yet the underlying molecular mechanisms are far from complete. Although the importance of SOX2 in cancer development and CCS are well recognized, the role of MTA3 in these processes is unknown. In this study, we used esophageal squamous cell carcinoma (ESCC) as a model system to demonstrate that MTA3 can repress both CCS and metastasis *in vitro* and *in vivo*. Mechanistically, by forming a repressive complex with GATA3, MTA3 downregulates SOX2OT, subsequently suppresses the SOX2OT/SOX2 axis, and ultimately represses CCS and metastasis. More importantly, MTA3^{low}/SOX2^{high} is associated with poor prognosis and could serve as an independent prognostic factor. These findings altogether indicate that MTA3/SOX2OT/SOX2 axis plays an indispensable role in CCS. Therefore, this axis could be potentially used in cancer stratification and serves as a therapeutic target.

INTRODUCTION

Cancer stem cells (CSCs) are a subpopulation of tumor cells capable of self-renewal and extensive proliferation. These properties make CSCs one of the driving forces in each of the cancer processes including progression, recurrence, and metastasis (Visvader and Lindeman, 2012). Accumulating evidence also suggests that CSCs play paramount roles in the development of therapeutic resistance (Nassar and Blanpain, 2016; Visvader and Lindeman, 2012). Given the fact that the overwhelming majority of cancer recurrences are due to the repopulation of cancer cells from CSCs, targeting CSCs would be an efficacious strategy in the development of treatments for therapeutic resistant cancers (Nassar and Blanpain, 2016). Thus, better understanding the underlying molecular mechanisms in both cancer development and maintenance of cancer stemness will provide strategies in designing new cancer treatments. An increasing body of evidence suggests that epigenetic changes play critical roles in the development of cancer stemness (Deshmukh et al., 2017). Epigenetic mechanisms such as histone modifications, DNA methylation, chromatin remodeling, and even changes in noncoding RNAs including long non-coding RNAs (lncRNAs) govern the epigenetic landscape that dictates the outcomes of cell fates without changing the DNA sequence (Leone and Santoro, 2016). Akin to embryonic stem cells, CSCs undergo similar epigenetic processes such as DNA methylation and chromatin remodeling (Deshmukh et al., 2017).

lncRNAs are a subgroup of RNA molecules that are more than 200 nucleotides in length without encoding any protein (Schmitt and Chang, 2016). It has been estimated that lncRNAs represent approximately 80% of the eukaryotic transcriptome, and the roles of lncRNAs have just started to be recognized (Schmitt and Chang, 2016). LncRNAs can have either tumor-suppressing or tumor-promoting activities, and genome-wide association studies of different tumor samples found that mutations and/or altered expressions of lncRNA could be responsible for both tumorigenesis and metastasis (Schmitt and Chang, 2016). Therefore, it has been suggested that the levels of some lncRNAs could be used as potential biomarkers and targeting lncRNAs could be developed into efficient cancer treatments (Bhan et al., 2017). SOX2OT (SOX2 overlapping transcript) is a lncRNA and directly involved in the regulation of SOX2, one of the master regulators crucial for both embryonic stem cells and cancer stemness (Li et al., 2018; Zhang et al., 2017). It has been noticed that not only is SOX2OT co-upregulated with SOX2 in multiple cancers including esophageal squamous cell carcinoma (Shahryari et al., 2014), lung squamous cell carcinoma (Hou et al., 2014), and breast cancer (Askarian-Amiri et al., 2014), but also upregulated SOX2OT and SOX2 also highly associate with poor outcome (Hou et al., 2014; Zhang et al., 2017). Of note, both SOX2OT and SOX2 are amplified in esophageal squamous cell carcinoma (ESCC) (Bass et al., 2009; Wang et al., 2017), although little is known about the regulation of the SOX2OT/SOX2 axis in this particular cancer.

[1]Department of General Surgery, The First Affiliated Hospital of Jinan University, Guangzhou, Guangdong 510632, China

[2]Institute of Precision Cancer Medicine and Pathology, Department of Pathology, Jinan University Medical College, Guangzhou, Guangdong 510632, China

[3]Cancer Research Center, Shantou University Medical College, Shantou, Guangdong 515041, China

[4]Department of Biomedical Sciences of Cells & Systems, Section Molecular Cell Biology and Radiation Oncology, University Medical Center Groningen, University of Groningen, Groningen 9700 AD, the Netherlands

[5]The Fourth Affiliated Hospital of Henan University of Science and Technology, Anyang, Henan 455001, China

[6]Department of Thoracic Surgery, Anyang Tumor Hospital, Anyang, Henan 455001, China

[7]Endoscopy Center, Affiliated Cancer Hospital of Shantou University Medical College, Shantou, Guangdong 515041, China

[8]Department of Thoracic Surgery, Affiliated Cancer Hospital of Shantou University Medical College, Shantou, Guangdong 515041, China

[9]Department of Emergency Medicine, University of Texas MD Anderson Cancer Center, Houston, TX 77030, USA

[10]Department of Endocrine Neoplasia and Hormonal Disorders, University of Texas MD Anderson Cancer Center, Houston, TX 77030, USA

[11]Department of Bio-Medical Sciences, Philadelphia College of Osteopathic

Continued

CellPress

By being involved in chromatin remodeling (Kumar and Wang, 2016), metastasis-associated proteins (MTAs) composed of MTA1, MTA2, and MTA3 (Toh and Nicolson, 2009) serve as master regulators in both physiological and pathological contexts (Ning et al., 2014). All family members of the MTA are associated with the NuRD complex to suppress a subset of target genes (Bowen et al., 2004; Manavathi et al., 2007; Yao and Yang, 2003). Although both MTA1 and MTA2 are generally considered as oncogenes mainly because they are capable of enhancing metastasis, MTA3 can serve as either a cancer repressor or an oncogene depending on cancer types (Ning et al., 2014). MTA3 was initially discovered as an estrogen-dependent gene that forms a distinct complex with Mi-2/NuRD and possesses strong transcription repressing activity on Snai1, leading to the upregulation of E-cadherin, and subsequently inhibits invasive growth of breast cancer cells (Zhang et al., 2006b). In addition, downregulation of MTA3 is associated with poor prognosis in a variety of cancers, including gastroesophageal junction adenocarcinoma (Dong et al., 2013), endometrioid adenocarcinomas (Bruning et al., 2010), and brain glioma (Shan et al., 2015). On the other hand, upregulation of MTA3 in uterine non-endometrioid (Mylonas and Bruning, 2012) and non-small cell lung cancer (Li et al., 2013) is significantly correlated with poor prognosis. Of note, it has been suggested that MTA3-mediated epigenetic remodeling of chromatins may be involved in the regulation of cancer stemness (Liau et al., 2017).

In this study, we explored the roles and the underlying molecular mechanisms of MTA3 in ESCC based on the following reasons: (1) ESCC is one of the major cancers in the digestive tract (Dong et al., 2017b; Feng et al., 2014) with 26%–53% of patients showing lymph node metastasis (Kumagai et al., 2018); (2) it appears that MTA3 utilizes a totally different EMT-regulating mechanisms in ESCC. We found that, in ESCC cells, MTA3 inhibits cancer stemness and metastasis by targeting the SOX2OT/SOX2 axis.

RESULTS

Downregulation of MTA3 Correlates with Tumor Progression and Poor Prognosis in Human ESCC

To systematically explore the roles of MTA3 in cancer initiation and progression, we first examined the protein levels of MTA3 in different organs based on the dataset obtained from the Human Protein Atlas database (www.proteinatlas.org) and found that MTA3 is almost ubiquitously expressed. However, its expression is particularly high in the gastrointestinal (GI) digestive tract including esophagus (Figures S1A and S1B), suggesting that MTA3 may play more important roles in these tissues. Results from analyzing the dataset GSE26886 showed that compared with that in normal esophageal epithelium tissues (n = 19) the mRNA levels of MTA3 are significantly lower in multiple GI tract diseases including ESCC tissues (n = 9), esophagus adenocarcinoma (n = 21), and Barrett esophagus (n = 20) (p < 0.001 for all; Figure S1C). In addition, a different dataset (GSE23400) also showed lower MTA3 mRNA levels in high percentage tumors (35/51) compared with their paired normal adjacent tissues (p < 0.01; Figure 1A). We then conducted qRT-PCR to estimate the mRNA levels of *MTA3* in ESCC patient samples and found that compared with their paired normal adjacent tissues 10 of 15 ESCC tissues expressed lower levels of *MTA3* mRNA (Figure 1B). We also conducted western blot assays to compare the protein levels of MTA3 in ESCC cell lines with two immortalized normal esophageal epithelial cell lines, NE2 and NE3. Figure 1C shows that all cancer cell lines examined express lower levels of MTA3. This finding is also consistent with the notion that ESCC cell lines express lower levels of MTA3 than that of normal esophageal epithelium cells (dataset GSE23964) (Figure S1D). These data altogether suggest that MTA3 may play some anti-cancer roles in ESCC.

To determine the clinical relevance of MTA3 in ESCC, we conducted immune-histochemical analyses to compare the protein levels of MTA3 in 125 ESCC tissues with their paired normal adjacent tissues and found that MTA3 is significantly lower in ESCC tissues (p < 0.001; Figure 1D). In addition, according to the receiver operating characteristic (ROC) curve (Figure 1E) with an optimal cutoff point of 4.25 (H-score) we found that 62.4% (78 of 125) of ESCC tissues versus only 12.5% (16 of 125) adjacent normal tissues had lower levels of MTA3. Furthermore, correlation analyses revealed that the protein levels of MTA3 are inversely correlated with both tumor depth (p = 0.011; Table S1) and advanced clinical stages (p = 0.033; Table S1). More importantly, Kaplan-Meier analyses showed that patients with ESCC with a lower level of MTA3 are associated with poorer prognosis (p = 0.001; Figure 1F) and multivariate Cox regression analyses showed that MTA3 can serve as an independent prognostic factor for overall survival of patients with ESCC (hazard ratio [HR], 2.717; 95% confidence interval [CI], 1.333–5.537, p = 0.006; Table S2). Finally, gene set enrichment analysis (GSEA) found that, compared with the paired normal adjacent tissues, the signature that negatively correlated with MTA3 is enriched in ESCC tissues (dataset

Medicine, 4170 City Avenue, Philadelphia, PA 19131, USA

[12]Key Laboratory of Epigenetics and Oncology, Research Center for Preclinical Medicine, Southwest Medical University, Luzhou, Sichuan 646000, China

[13]Research Centre of Translational Medicine, The Second Affiliated Hospital of Shantou University Medical College, Shantou, Guangdong 515063, China

[14]These authors contributed equally

[15]Lead Contact

*Correspondence:
zhoufuyou007@163.com
(F.Z.),
haozhang@jnu.edu.cn (H.Z.)
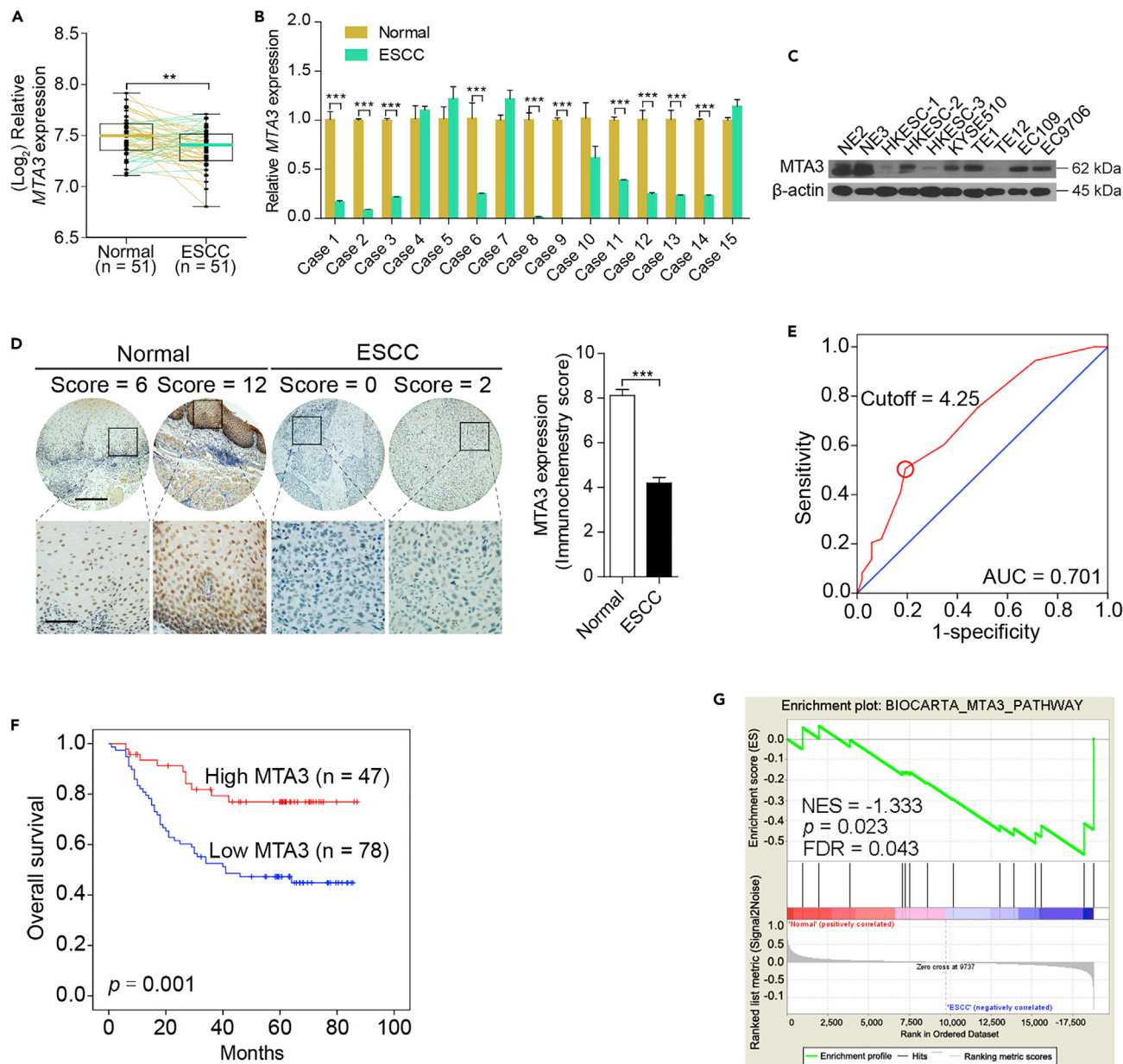https://doi.org/10.1016/j.isci.2019.11.009

Figure 1. Downregulation of MTA3 Correlates with Poor Prognosis in Human ESCC

(A) The mRNA levels of *MTA3* in the ESCC dataset GSE23400.

(B) The mRNA levels of *MTA3* in 15 human ESCC specimens and their paired normal adjacent tissues.

(C) Western blot analysis of MTA3 in a panel of ESCC cell lines and two immortalized esophageal epithelial cell lines. β-Actin is used as a loading control.

(D) Immunohistochemistry (IHC) of MTA3 in 125 human ESCC tissues and their paired adjacent normal tissues (left panel). The immunohistochemistry score of MTA3 in ESCC (filled bar) and the paired normal adjacent (open bar) tissues (right panel). Scale bars: upper panels, 400 μm; lower panels, 100 μm.

(E) Receiver operating characteristic (ROC) curve analysis to determine the cutoff score for low expression of MTA3.

(F) Kaplan-Meier curves compared the overall survival in patients with ESCC with high and low protein levels of MTA3.

(G) GSEA plots of enrichment of BIOCARTA_MTA3_PATHWAY in normal adjacent tissues versus ESCC specimens in the GSE23400 dataset. FDR q, false-discovery rate q value; NES, normalized enrichment score.

Data were shown as the means from at least three independent experiments or representative data. Error bars indicate SEM. **p < 0.01, ***p < 0.001 by Student's t test. See also Figure S1, Table S1, and Table S2.

GSE23400) (p = 0.023, false discovery rate [FDR] = 0.043; Figure 1G). Taken together, these data suggest that MTA3 might possess a repressive role in ESCC progression.

MTA3 Suppresses ESCC Cell Metastasis and Stemness

To gain insights into the potential repressive role of MTA3 in ESCC progression, we conducted GSEA on the dataset GSE23400 to explore the downstream signaling of MTA3 and found that MTA3 expression is inversely related to the metastatic signatures (p = 0.024, FDR = 0.035; Figure S2A). We chose four cell lines to examine the effect of MTA3 on the metastasis makers and found that knockdown MTA3 in ESCC cells leads to significant reduction and induction of the epithelial marker (E-cadherin) and mesenchymal markers (N-cadherin and vimentin), respectively (Figure S2B). On the other hand, overexpression of MTA3 showed the exact opposite effects on these markers (Figure S2B). These results support the notion that MTA3 may be involved in the regulation of ESCC cell metastasis. In addition, MTA3 knockdown not only makes the actin filaments in cells more elongated stress fibers but more cells also lost their cell-cell contacts (Figure S2C). The fluorescent phalloidin staining results also showed that overexpression of MTA3 altered the shape of cells from spindle-like, fibroblastic morphology to a cobblestone-like appearance (Figure S2C). The more flexible cytoskeleton of neoplastic is expected to favor cell migration through the trans-well, and indeed the trans-well assays showed that more MTA3-depleted cells migrated through the membrane (p < 0.05 for all; Figure S2D). In contrast, MTA3 overexpression suppressed both ESCC cell invasion and migration (p < 0.001 for both; Figure S2D). These data collectively demonstrated that MTA3 possesses a repressive role in ESCC cell metastasis.

Before conducting experiments to determine the MTA3's effect on ESCC metastasis in vivo, GSEA analyses on two separate datasets were conducted to determine the effect of MTA3 on tumor cell proliferation and lymph node invasion. We found that (1) MTA3 expression was inversely related to cell proliferation (dataset GSE23400) (p = 0.027, FDR = 0.032; Figure S3A) and (2) ESCC tissues with low MTA3 activity are more intend to have lymph node metastasis (dataset GSE47404) (p = 0.032, FDR = 0.041; Figure S3B). Then we estimated the effect of MTA3 on ESCC cells using the in vivo animal model. Figures S3C and S3D showed that tumors derived from EC9706 and EC109 cells were not only larger but also heavier when MTA3 is knocked down by shRNA (p < 0.01 for all). On the other hand, the tumors derived from EC9706 and HKESC-1 cells were smaller and lighter when MTA3 is overexpressed (p < 0.01 for both; Figures S3E and S3F). These results indicate that MTA3 can repress ESCC cell proliferation in vivo. In addition and consistent with the in vitro data, epithelial marker (E-cadherin) and mesenchymal markers (N-cadherin and Vimentin) in tumors derived from ESCC cells were significantly decreased and increased, respectively, when MTA3 was knocked down (Figure S3G). This suggests that MTA3 can repress ESCC cell metastasis in vivo. To further substantiate this finding, the EC9706 and TE1 cells with or without shMTA3 transfection were labeled with luciferase and injected into the flanks of nude mice (Figures 2A, S3H, and S3I). The expression of luciferase enabled us to monitor the tumor cell dissemination and inguinal lymph node metastasis. We found that depletion of MTA3 promoted inguinal lymph node metastasis (Figures 2B, 2C, and S3J), which is further substantiated by hematoxylin and eosin (H&E) staining (Figure 2F). Finally, when these cells were injected into the tail vein of nude mice, more ESCC cells in the MTA3 knockdown group were found in the lungs (Figure 2D and 2E), which is substantiated with results of H&E staining (Figure 2G). These findings altogether lead us to conclude that MTA3 plays an important repressive role in ESCC cell proliferation and metastasis in vivo.

Since merging evidence points toward a central role of MTA3 in epithelial to mesenchymal transition (EMT) by targeting Snai1 (Fujita et al., 2003), we decided to determine whether MTA3 is involved in the regulation of Snai1 in ESCC cells. To do so, we conducted qRT-PCR to estimate the mRNA levels of Snai1 and the other EMT-related transcriptional factors including Twist 1, Twist2, and ZEB1 in three ESCC cell lines (EC9706, EC109, and TE1) with or without MTA3 knockdown. As shown in Figures S4A–S4D, knockdown MTA3 in these cells has no effect on any of these factors in both RNA and protein levels. Then a luciferase reporter plasmid under the control of promoter of the Snai1 gene was transfected to these three cell lines with or without MTA3 knockdown. Consistent with the qRT-PCR results, knockdown MTA3 has no effect on luciferase activity under the control of the Snai1 promoter (Figures S4E–S4G). Therefore, we assumed that the effect of MTA3 on ESCC metastasis is through regulatory mechanisms other than these EMT regulators. CSCs are a small subpopulation of cells in the cancer tissue and play important roles in every aspect of cancer development, including initiation, progression, and metastasis. To explore whether MTA3 plays any role in CSCs, we conducted a GSEA on dataset GSE23400 and found that MTA3 is inversely associated
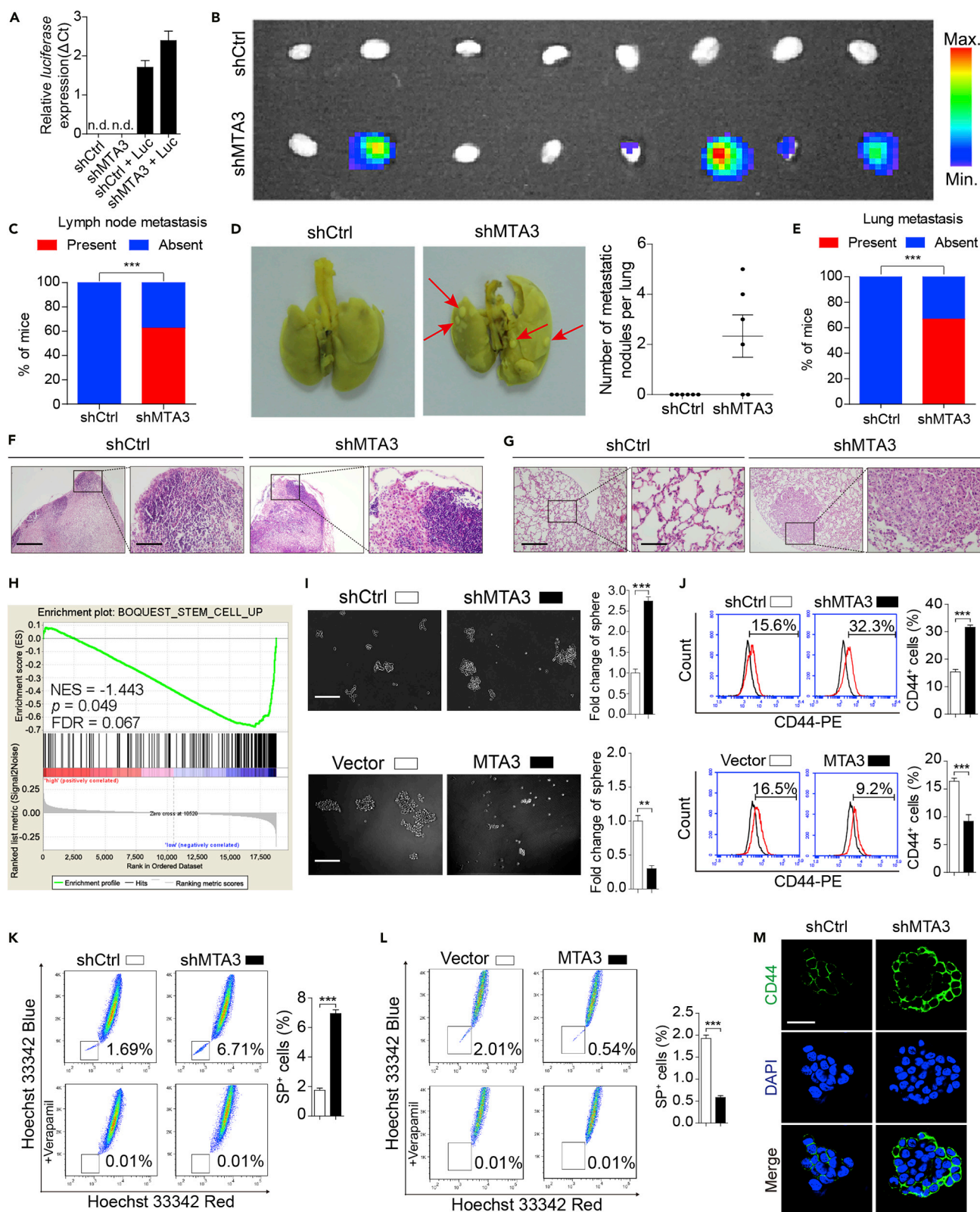
Figure 2. MTA3 Suppresses Metastasis and Stemness of ESCC Cells

(A) EC9706 cells transfected with shMTA3 or shCtrl were infected with lentiviruses carrying luciferase and then subjected to RNA extraction followed by qRT-PCR analysis of luciferase gene.

(B–G) The EC9706 cells with or without MTA3 depletion were infected with recombinant lentiviruses carrying luciferase and injected subcutaneously into the flanks of nude mice (n = 8). The inguinal lymph nodes of the animals were extracted and analyzed for the presence of metastatic cells by bioluminescence imaging (B), and proportion of inguinal lymph nodes metastasis in the nude mice (C). EC9706 cells transfected with shMTA3 or shCtrl were injected intravenously through the tail vein of nude mice (n = 6). Representative images of lung metastasis were shown (D, left panel), numbers of metastatic nodules per lung in the nude mice (D, right panel), and proportion of lung metastasis in the nude mice (E). (F) The inguinal lymph nodes were analyzed by H&E. Scale bars: left panels, 400 μm; right panels, 100 μm. (G) Lung architecture is shown by H&E. Scale bars: left panels, 400 μm; right panels, 100 μm.

(H) GSEA plots of enrichment of BOQOEST_STEM_CELL_UP signatures in MTA3^{High} tumors versus MTA3^{Low} tumors in the GSE23400 dataset.

(I) Representative images of spheres formed by EC9706 cells with MTA3 depleted (upper panel) or overexpressed (lower panel). Histograms showing the fold change in the number of spheres formed by EC9706 cells with MTA3 depleted (upper right panel) or overexpressed (lower right panel). Scale bars: 200 μm.

(J–L) (J) Flow cytometry analysis of the CD44$^+$ population in EC9706 cells with MTA3 depleted (upper panel) or overexpressed (lower panel). Histograms showing the proportion of CD44$^+$ cells in EC9706 cells with MTA3 depleted (upper right panel) or overexpressed (lower right panel). (K and L) Hoechst 33342 dye exclusion assay of the SP$^+$ population in EC9706 cells with MTA3 depleted (K) or overexpressed (L). Histograms showing the proportion of SP$^+$ cells in EC9706 cells with MTA3 depleted (K, right panel) or overexpressed (L, right panel).

(M) Representative images of immunofluorescence for CD44 proportion in EC9706 cells with MTA3 depleted. Scale bars: 40 μm.

Data are shown as the means of three independent experiments or representative data. Error bars indicate SEM. **p < 0.01, ***p < 0.001 by Student's t test or chi-square test, where appropriate. See also Figures S2–S5.

with stemness signatures (p = 0.049, FDR = 0.067; Figure 2H). We then estimated MTA3's effect on mammosphere formation and found that knockdown and overexpression of MTA3 significantly (p < 0.01) increased and decreased the number of mammospheres, respectively (Figures 2I and S5A), suggesting that MTA3 possesses property against ESCC cancer stemness. To substantiate these findings, we estimated MTA3's effects on the CD44$^+$ and side population (SP) cells (Chen et al., 2013) and found that depletion of MTA3 significantly (p < 0.001) increased the proportion of both CD44$^+$ (Figures 2J and S5B) and SP$^+$ (Figures 2K and S5C) cells, whereas overexpression of MTA3 decreased the proportion of both CD44$^+$ (Figures 2J and S5B) and SP$^+$ cells (Figure 2L). Finally, CD44 increased dramatically in ESCC cells when MTA3 is knocked down (Figures 2M and S5D). Of note, the role of MTA3 in ESCC cancer stemness was supported by the findings in other tumors, including head and neck squamous cell carcinoma (HNSCC), oral squamous cell carcinoma (OSCC), breast invasive carcinoma (BRCA), and pancreatic adenocarcinoma (PAAD) datasets (Figures S5E–S5H).

MTA3 Downregulates SOX2 and SOX2OT Simultaneously

To understand the mechanism in MTA3-regulated ESCC cancer stemness, we conducted a stemness PCR array and found that MTA3 knockdown leads to certain stemness-related genes to be up- or down-regulated, and 11 of them were elevated more than 1.5-fold (Figure S6A). Results from analyzing these 11 genes in the Cancer Genome Atlas (TCGA) database suggested that CHEK1, SOX2, and TAZ were significantly upregulated in ESCC tissues (Figure S6B). We then conducted qRT-PCR on these three genes and found that only SOX2, not the other two, is significantly up- and down-regulated by MTA3 depletion and overexpression, respectively (Figures S6C and S6D). In addition, western blot assays also confirmed that MTA3 downregulates SOX2 in ESCC cells (Figure S6E). Given the pivotal roles of SOX2 in both embryonic and cancer stemness (Bass et al., 2009; Li et al., 2018), we examined MTA3's effect on SOX2 expression. However, luciferase reporter assays showed that MTA3 has no regulatory effect on SOX2 promoter (Figures S6F and S6G), suggesting that MTA3 could regulate SOX2 indirectly.

SOX2 overlapping transcript (SOX2OT) is a lncRNA located in the intron of the SOX2 gene (Li et al., 2018) and transcribed in the same orientation of SOX2. It has been reported that SOX2OT is co-upregulated with SOX2 in ESCC cells (Shahryari et al., 2014), and upregulation of SOX2OT and SOX2 is involved in the regulation of cancer stemness (Li et al., 2018). Mechanistically, SOX2OT upregulates SOX2 by serving as a competing endogenous RNA (ceRNA) to sequester specific microRNA (miRNA) and subsequently counteract miRNA-mediated SOX2 downregulation (Li et al., 2018). We decided to determine if MTA3 represses SOX2 expression via targeting SOX2OT. We found that MTA3 knockdown and overexpression significantly (p < 0.01) up- and down-regulated both SOX2OT and SOX2, respectively (p < 0.01, Figures 3A–3D). Finally, we conducted luciferase reporter assays to determine MTA3's regulatory role in SOX2OT transcription. Figure 3E demonstrated that MTA3 is capable of repressing SOX2OT promoter activity because of depletion and overexpression of MTA3 significantly up- and down-regulated the reporter activity, respectively (p < 0.001 for both). Together, these data suggest that, in ESCC cells, MTA3 indirectly downregulates SOX2 by targeting SOX2OT.
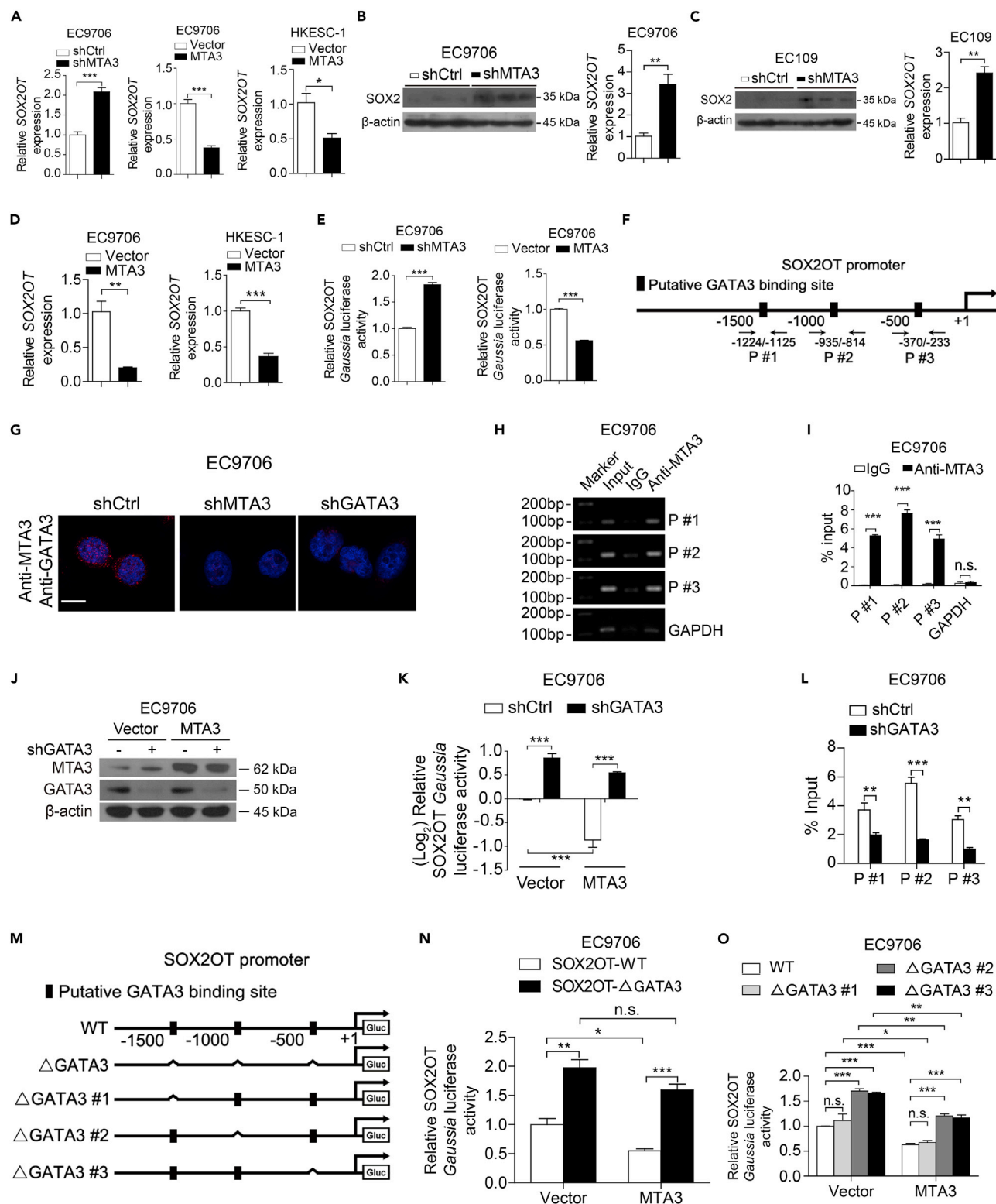
Figure 3. MTA3 Inhibits SOX2OT Transcription Depending on GATA3

(A) QRT-PCR of SOX2OT in EC9706 cells with MTA3 depletion or MTA3 overexpression and in HKESC-1 cells with MTA3 overexpression.

(B–D) Western blot of SOX2 and qRT-PCR of SOX2OT in tumors derived from EC9706 (B) and EC109 (C) cells with MTA3 depletion, or EC9706 cells and HKESC-1 cells with MTA3 overexpression (D).

Figure 3. Continued

(E) SOX2OT *Gaussia* luciferase reporter activity in EC9706 cells with MTA3 depletion or overexpression.

(F) Schematic structure of the SOX2OT promoter and positions of ChIP primers.

(G) Proximity Ligation Assay (PLA) detection of MTA3-GATA3 interaction. EC9706 cells transfected with the indicated shRNAs were subjected to PLA using antibodies against MTA3 or GATA3. Scale bars: 10 μm.

(H and I) ChIP assay using antibodies against MTA3 or IgG. Semi-quantitative PCR (H) and qPCR (I) to detect the enriched DNA fragments in the SOX2OT promoter region.

(J) Western blot of GATA3 in MTA3 overexpressed EC9706 cells transfected with shGATA3-expressing plasmid. β-Actin is shown as a loading control.

(K) SOX2OT luciferase reporter activity in EC9706 cells transfected with the MTA3 or shGATA3 plasmids.

(L) ChIP assay was performed in EC9706 cells with GATA3 depletion using antibodies against MTA3 or IgG, and qPCR was used to detect the enriched DNA fragments in the SOX2OT promoter region.

(M) Schematic structure of deletion-mutation reporters of the SOX2OT promoter.

(N and O) The SOX2OT promoter-reporter and mutations ΔGATA3 (N) or in GATA3-binding site 1 (ΔGATA3 #1), GATA3-binding site 2 (ΔGATA3 #2), GATA3-binding site 3 (ΔGATA3 #3) (O). The relative SOX2OT Gaussia luciferase reporter activities 72 h after transfection.

Data are shown as the means of three independent experiments or representative data. Error bars indicate SEM, n.s., not statistically significant; *p < 0.05, **p < 0.01, ***p < 0.001 by Student's t test or a one-way ANOVA with post hoc intergroup comparisons, where appropriate. See also Figures S6 and S7, and Table S3.

MTA3 Is Recruited by GATA3 to Repress SOX2OT Transcription

Although MTA3 harbors a putative DNA-binding domain, there is no evidence indicating that MTA3 can interact with DNA directly (Kumar and Wang, 2016). Since it has been reported that MTA3 can serve as a transcriptional repressor by complexing with GATA3 (Si et al., 2015), we conducted bioinformatics analyses using PROMO (http://alggen.lsi.upc.es/cgi-bin/promo_v3/promo/promoinit.cgi?dirDB=TF_8.3) and JAS-PAR (http://jaspar.genereg.net/) and found three potential GATA3-binding sites in the promoter region of SOX2OT gene (Figure 3F). We then conducted a simple duo-link assay and found that MTA3 is very likely to complex with GATA3 in ESCC cells (Figure 3G). To determine whether MTA3 is recruited to the promoter of SOX2OT, we performed chromatin immunoprecipitation (ChIP) assays using an antibody against MTA3 and the precipitated DNA was amplified with different pairs of primers (Figure 3F). Results from both semi-quantitative PCR (Figure 3H) and qPCR (Figures 3I and S7A) demonstrated that MTA3 is recruited to the promoter region of the SOX2OT gene by GATA3 because knockdown of GATA3 abolished MTA3's repressive effect on SOX2OT and inhibited the MTA3's occupation on the promoter region of SOX2OT (Figures 3J–3L, S7B, and S7C). To determine which GATA3-binding site(s) is responsible for MTA3 recruitment, we conducted luciferase reporter assays with one, two, or three potential GATA3 being deleted (Figure 3M) from the SOX2OT promoter. Figure 3N shows that MTA3 failed to repress SOX2OT promoter activity when these potential GATA3 sites were deleted. In addition, potential GATA3-binding site #1 is likely to be not involved in MTA3 recruitment because deletion of this site has no effect on MTA3-mediated repression. However, sites #2 and #3 are likely to be responsible for the recruitment of GATA3/MTA3 complex because deleting either of them reduced MTA3-mediated repression significantly (p < 0.001, Figure 3O). These results collectively demonstrated that, in ESCC cells, MTA3 is recruited by GATA3 to inhibit SOX2OT expression.

MTA3 Represses Metastasis and Cancer Stemness by Targeting the SOX2OT/SOX2 Axis

To determine if MTA3-repressed cancer stemness is mediated by the SOX2OT/SOX2 axis, we first examined the role of SOX2OT in MTA3-regulated EMT, invasion, and stemness by analyzing the changes of specific markers in the presence or absence of SOX2OT. Figure 4A showed that SOX2OT was successfully knocked down by locked nucleic acid (LNA)-modified antisense oligonucleotides (GapmeRs), which is referred as SOX2OT AS. As expected, knockdown of SOX2OT leads to a reduced level of SOX2. Figure 4A also showed that knockdown of MTA3 not only leads to higher levels of both SOX2 and SOX2OT but also altered the EMT and stemness markers accordingly. Of note, MTA3-depletion-mediated SOX2 upregulation is significantly reduced when SOX2OT is depleted, suggesting that SOX2OT plays a crucial role in MTA3-mediated SOX2 repression. We have also examined the effect of overexpression of either SOX2OT or MTA3 individually or in combination on SOX2 and specific markers. Figure 4B showed that overexpressed SOX2OT and MTA3 were able to up- and down-regulate SOX2, respectively. However, overexpressed SOX2OT is capable of counteracting MTA3-repressed SOX2 expression as well as the alteration of EMT and stemness markers. In addition, Figures 4C and 4D show that SOX2OT promotes both cell invasion and cancer stemness and MTA3 represses these processes by inhibiting SOX2OT. These observations are consistent with the effect of SOX2OT and MTA3 on the subpopulations of CD44^{+} and SP^{+} cells (Figure S8). More importantly, overexpressed MTA3 inhibited SOX2OT-induced inguinal lymph node
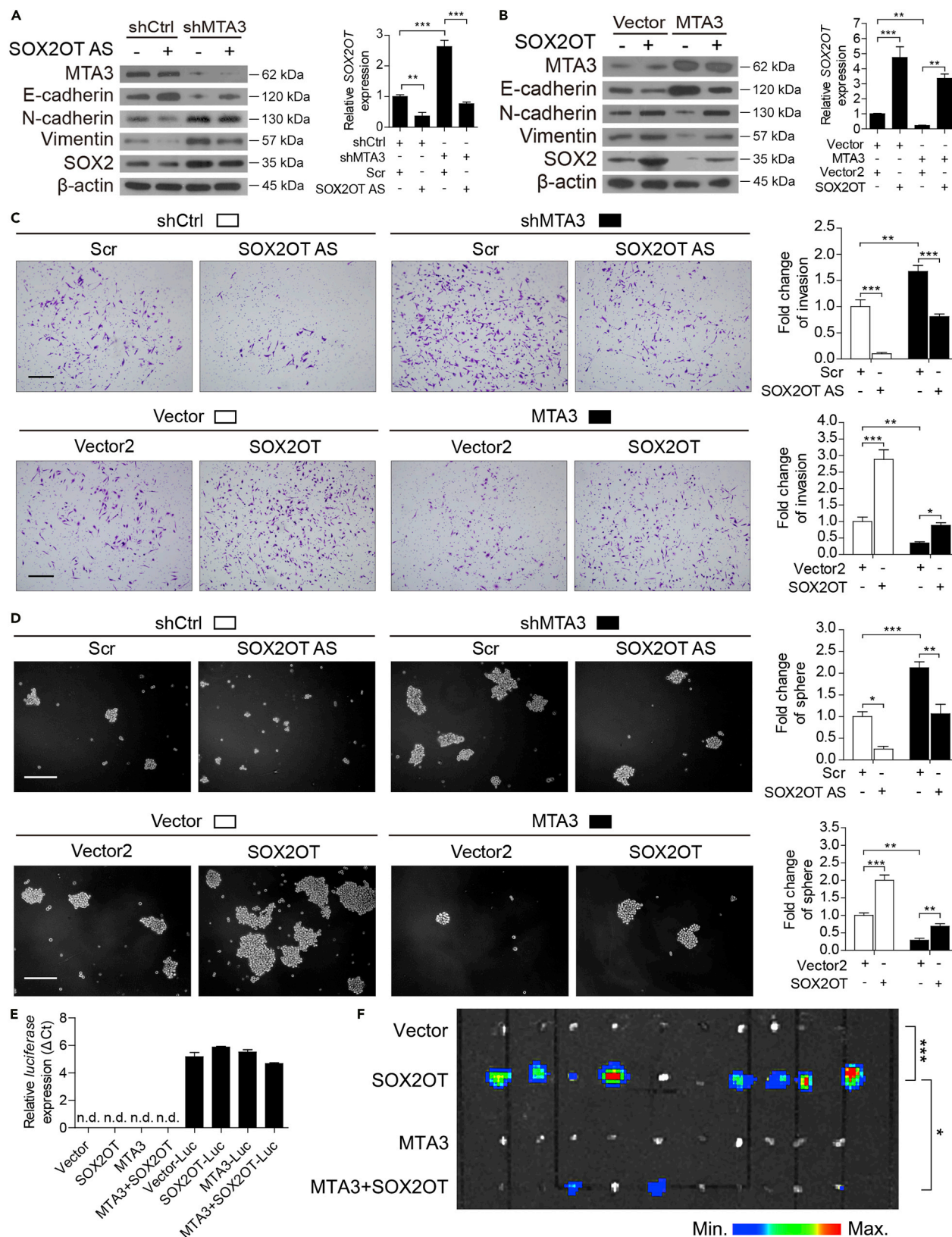
Figure 4. MTA3 Regulates ESCC Cell Metastatic Potential and Stemness via SOX2OT

(A and B) Western blot and qRT-PCR in EC9706 cells transfected with a combination of shMTA3 and SOX2OT AS oligo (A) or MTA3- and SOX2OT-expressing plasmid (B).

(C and D) The above-mentioned cells were subjected to the cell invasion assay (C) and sphere assay (D). Representative fields of the invaded cells, and sphere (left panels). Histograms with the fold change in the number of invaded cells and spheres formed by the indicated cells (right panels). Scale bars: 200 μm in (C) and (D).

(E) The indicated cells were infected with lentiviruses carrying luciferase and then subjected to RNA extraction followed by qRT-PCR analysis of luciferase gene. The inguinal lymph nodes were extracted and analyzed for the presence of metastatic cells by bioluminescence imaging.

(F) EC9706 cells transfected with a combination of MTA3- and SOX2OT-expressing plasmid were infected with recombinant lentiviruses carrying luciferase and injected subcutaneously into the flanks of nude mice (n = 10). The inguinal lymph nodes of the animal were extracted and analyzed for the presence of metastatic cells by bioluminescence imaging.

Data were shown as the means of three independent experiments or representative data. Error bars indicate SEM. *p < 0.05, **p < 0.01, ***p < 0.001 by one-way ANOVA with post hoc intergroup comparisons or chi-square test, where appropriate. See also Figure S8.

metastasis (Figures 4E and 4F). These data altogether demonstrated that, in ESCC cells, MTA3 represses cancer metastasis and stemness by targeting the SOX2OT/SOX2 axis.

MTA3-Repressed SOX2OT/SOX2 Axis Is Significant in the Outcomes of Patients with ESCC Cancer

We conducted qRT-PCR to measure the mRNA levels of MTA3, SOX2OT, and SOX2 in 32 patients with ESCC, and a Pearson's correlation analysis showed a significant negative correlation between MTA3 and SOX2OT (r = −0.408, p = 0.021; Figure 5A) or SOX2 (r = −0.393, p = 0.026; Figure 5B). In addition, the level of SOX2OT is positively correlated with the mRNA level of SOX2 (r = 0.874, p < 0.001; Figure 5C). We have also conducted immunohistochemistry (IHC) to estimate SOX2 in a separate cohort of 125 patients with ESCC. Based on the ROC curve analysis, the samples with IHC score ≥4.5 were categorized into the high-SOX2 group and those with IHC scores <4.5 were in the low-SOX2 group (Figure 5D). Kaplan-Meier analyses found that patients with ESCC in the high-SOX2 group had a poorer prognosis than those in the low-SOX2 group (p < 0.001; Figure 5E). Correlation analyses also found that tumors with low levels of MTA3 were more likely to have high levels of SOX2 (p < 0.01; Figure 5F). These patients with ESCC were stratified into different groups based on the levels of MTA3 and SOX2. Kaplan-Meier analyses found that overall survival of patients in the low-MTA3/high-SOX2 group is significantly worse than those in the high-MTA3/low-SOX2 (p < 0.001; Figure 5G), high-MTA3/low-SOX2, high-MTA3/high-SOX2, and low-MTA3/low-SOX2 (p < 0.001; Figure 5H) groups. Finally, multivariate Cox regression analyses found that low-MTA3/high-SOX2 (HR, 3.273; 95% CI, 1.815 to 5.901, p = 0.000) can be used as independent prognostic indicators in ESCC patient prognosis (Table 1). These results indicate that the MTA3-targeted SOX2OT/SOX2 axis plays an important role in not only cancer stemness but also ESCC cancer patient outcomes.

Targeting the MTA3-SOX2OT/SOX2 Axis Represses Cancer Stemness

We decided to examine the roles of MTA3, SOX2OT, and SOX2 individually or in combination in cancer stemness in animal models and explore the potential of targeting MTA3-mediated SOX2OT/SOX2 axis as therapeutic strategies. To do so, we first used EC9706 cells to establish overexpression of MTA3 or SOX2 individually or in combinations (Figure 6A) as well as knockdown of MTA3 or SOX2 by specific shRNA individually or in combination (Figure 6B). These cells were subcutaneously injected into nude mice, and the tumor volumes were monitored weekly for 4–5 weeks. The animals were sacrificed at the end of the experiment, and the tumors were dissected and weighed. Figures 6C and 6D show that the tumors derived from the cells with MTA3 overexpression were significantly smaller/lighter and the tumors derived from the cells overexpressing either SOX2OT or SOX2 were significantly bigger/heavier. In addition, the size/weight of tumors derived from the cells overexpressing MTA3 with either SOX2OT or SOX2 was bigger/heavier than that with MTA3 overexpression alone but smaller/lighter than that with either SOX2OT or SOX2 overexpression. On the other hand, the tumors derived from the cells with MTA3 and SOX2 knockdown were bigger/heavier and smaller/lighter, respectively. The size/weight of the tumors derived from the cells with knockdown of both MTA3 and SOX2 was similar to that of the control (Figure 6E). Furthermore, results from IHC revealed that the effect of MTA3 on stemness markers was attenuated by overexpression of either SOX2OT or SOX2 (Figures 6F and 6G). Moreover, shRNA-mediated SOX2 depression markedly abolished the MTA3 depletion-induced alterations of stemness markers (Figure 6H). More importantly, flow cytometry analyses showed that the decrease of CD44$^+$ and SP$^+$ cells by MTA3 overexpression was overcome by overexpression of SOX2OT or SOX2 (Figures 6I and 6J), whereas the MTA3 silencing-induced CD44$^+$ and SP$^+$ subpopulation was hampered by SOX2 depletion (Figure 6K). These findings collectively support the
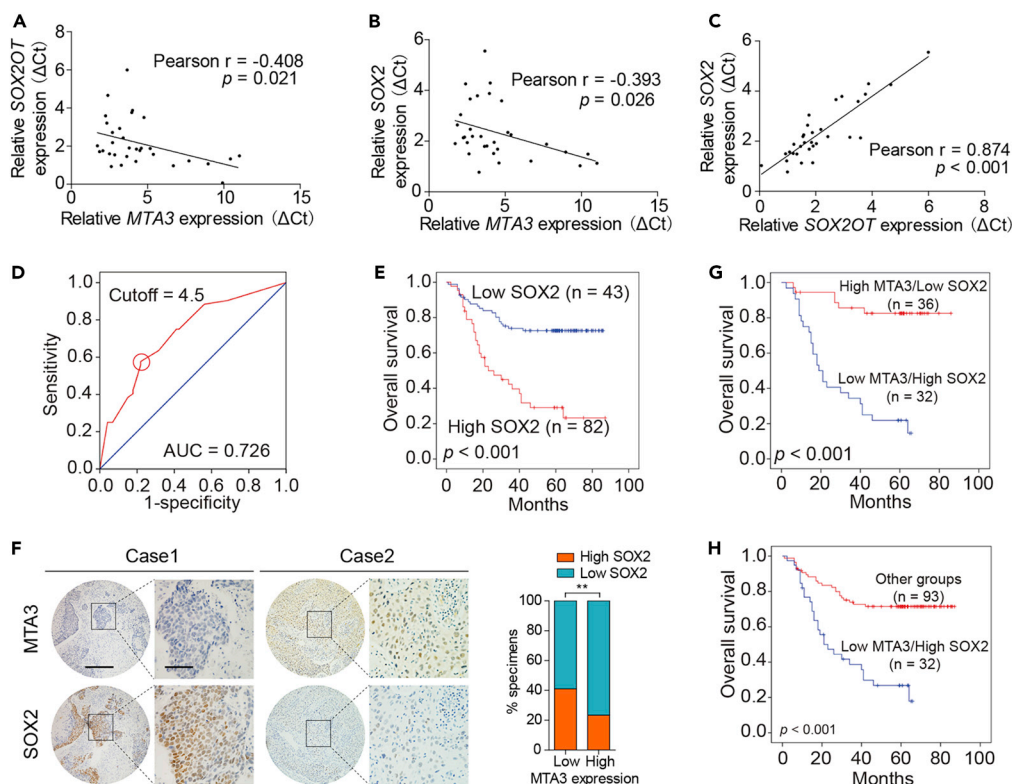
Figure 5. The Dysregulated MTA3-SOX2OT-SOX2 Axis Is Associated with Metastasis and Poor Prognosis

(A–C) Pearson's correlations of *MTA3* and *SOX2OT* (A), *MTA3* and *SOX2* (B), *SOX2OT* and *SOX2* (C) in 32 primary human ESCC specimens.

(D) ROC curve analysis was performed to determine the cutoff score for the overexpression of SOX2.

(E) Kaplan-Meier curves compared the overall survival in patients with ESCC with high and low protein levels of SOX2.

(F) Correlation of MTA3 and SOX2 IHC score in 125 primary human ESCC specimens (left panel). Percentage of samples showing low or high SOX2 ratio relative to the levels of MTA3 in 125 cases of human ESCC samples (right panel). Scale bars: left panels, 400 μm; right panels, 100 μm.

(G and H) Overall survival in patients with ESCC with tumors with low-MTA3/high-SOX2 (G) or low-MTA3 and other groups (H). **p < 0.01 by chi-square test.

notion that MTA3 suppresses ESCC stemness *in vivo* through the SOX2OT/SOX2 axis and SOX2OT is essential for MTA3's repressive function of cancer stemness.

DISCUSSION

The biological and clinical significance of the MTA family members in malignancies has been well established. The levels of these factors have even been proposed as potential diagnostic parameters, and targeting each one of the family members could be potential treatments for different cancers (Ning et al., 2014). However, unlike MTA1 and MTA2, which were mainly involved in cancer progression and metastasis, MTA3 possesses both tumor-suppressing and tumor-promoting properties depending on specific cancer types (Ning et al., 2014). We found that, by targeting the SOX2OT/SOX2 axis, MTA3 represses metastasis and cancer stemness in ESCC. Further mechanistic studies demonstrated that MTA3 is recruited by GATA3 to repress SOX2OT transcription. Given the fact that alterations of MTA3 as well as its downstream SOX2OT/SOX2 axis highly correlate with clinical outcomes and the predictability of prognosis, the levels of MTA3, SOX2, and SOX2OT, especially low-MTA3/high-SOX2, could be used as diagnostic parameters, and targeting either MTA3 or the SOX2/SOX2OT axis could be potential therapeutic strategies in ESCC treatment.

Different research groups including ours have extensively studied the well-established regulatory role of MTA3 in EMT (Ning et al., 2014). We found that MTA3 is significantly downregulated in gastroesophageal

Variables	Univariate Analysis	p Value	Multivariate Analysis	p Value
	HR (95% CI)		HR (95% CI)	
Gender				
Male versus Female	1.421 (0.730–2.766)	0.301	1.477 (0.743–2.935)	0.266
Age				
≥60 versus <60	1.526 (0.880–2.645)	0.132	1.547 (0.883–2.711)	0.128
Histologic grade				
Poor/Moderate versus Well	1.586 (0.879–2.860)	0.126	1.833 (0.938–3.582)	0.076
Tumor size				
≥5 cm versus < 5 cm	1.237 (0.698–2.191)	0.466	0.975 (0.544–1.751)	0.934
Tumor depth				
T_3/T_4 versus T_1/T_2	3.332 (1.200–9.246)	0.021	1.529 (0.490–4.775)	0.465
Lymph node metastasis				
Positive versus Negative	1.484 (0.844–2.612)	0.170	0.654 (0.327–1.307)	0.229
Stage				
III versus I/II	3.940 (1.774–8.750)	0.001	3.297 (1.253–8.675)	0.016
Combination of MTA3 and SOX2				
Low MTA3/High SOX2 versus Others	3.738 (2.151–6.498)	0.000	3.273 (1.815–5.901)	0.000

Table 1. Univariate and Multivariate Cox Proportional Hazards Model Predicting Survival in ESCC
ESCC, esophageal squamous cell carcinoma; HR hazard ratio; CI, confidence interval.

junction adenocarcinoma and its downregulation is highly associated with upregulated Snai1 and enhanced EMT (Dong et al., 2013). Accordingly, MTA3 represses ESCC metastasis and cancer stemness. This finding is in line with the fact that MTA3 is capable of inhibiting the initiation of primitive hematopoiesis in vertebrate embryos (Li et al., 2009), repressing EMT in breast cancer cells (Fujita et al., 2003), and suppressing Wnt4 pathway in mammary epithelial cells (Zhang et al., 2006a), implicating a role for MTA3 in regulation of stem cell properties. More importantly, the results from our gain-of-function and loss-of-function experiments demonstrated that, instead of targeting Snai1, Twist1, Twist2, and ZEB1, MTA3 inhibits ESCC metastasis and cancer stemness by repressing SOX2OT/SOX2 axis. To our knowledge, this is the first report about MTA3's regulatory role in cancer stemness in ESCC.

Similar to SOX2, SOX2OT is highly expressed in embryonic stem cells and downregulated upon the induction of differentiation (Shahryari et al., 2014). The dysregulation of SOX2OT and SOX2 have been noticed in some cancers, including esophageal squamous cell carcinoma (Shahryari et al., 2014), lung squamous cell carcinoma (Hou et al., 2014), and breast cancer (Askarian-Amiri et al., 2014). Moreover, SOX2OT and SOX2 are co-upregulated in breast cancer cell lines during suspended culturing with enhanced CSC-like properties (Askarian-Amiri et al., 2014). Both SOX2OT and SOX2 have also been reported to promote cancer cell metastatic potential (Li et al., 2018). Although the roles of SOX2OT in SOX2 regulation are not well established, it appears that SOX2OT regulates SOX2 transcriptionally (Li et al., 2018; Zhang et al., 2017). In pancreatic ductal adenocarcinoma, the transcription regulator Yin Yang-1 (YY1) occupies the SOX2OT promoter and suppresses its transcription (Zhang et al., 2017). Androgen receptor (AR) binds to the promoter of SOX2OT and modulates RNA polymerase II-driven SOX2OT expression in mouse forebrains and embryonic neural stem cells (Tosetti et al., 2017). SOX2OT is also regulated by microRNAs such as miR-211 (Shafiee et al., 2016). Gene amplification and promoter hypomethylation of SOX2OT gene are strongly associated with higher expression of SOX2OT (Brennan et al., 2017; Hou et al., 2014). We found that MTA3 is recruited by GATA3 to the promoter region of SOX2OT and subsequently represses SOX2OT transcription. Therefore, low levels
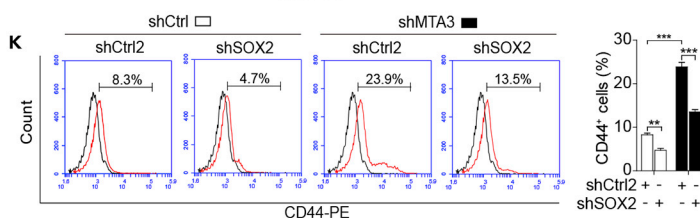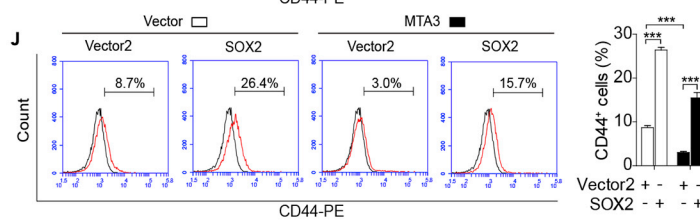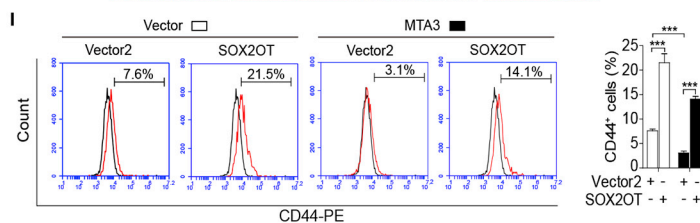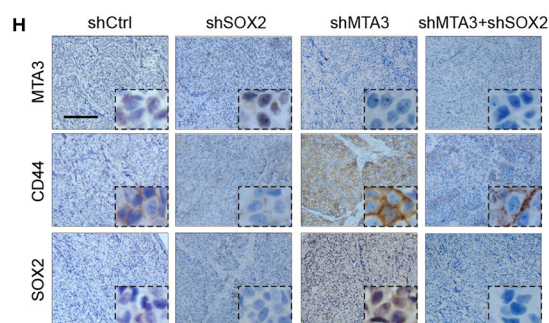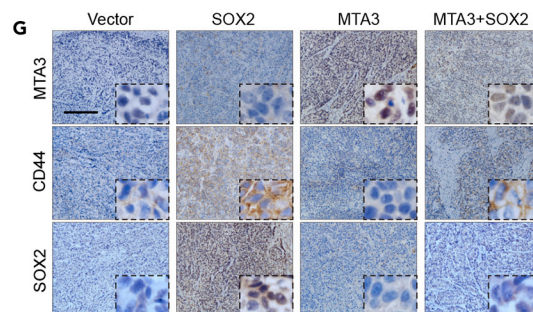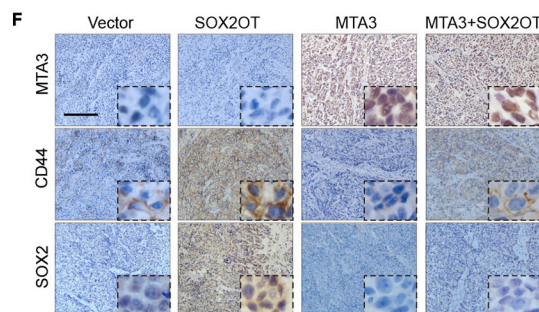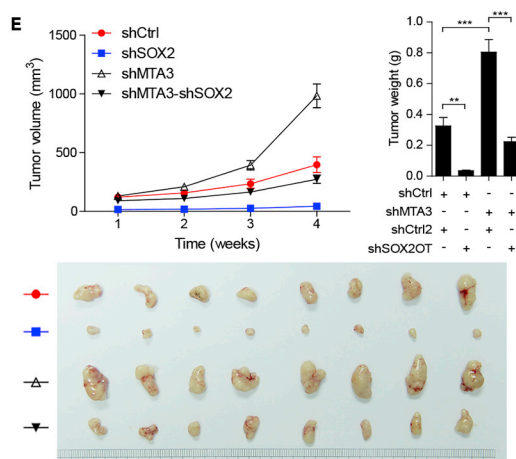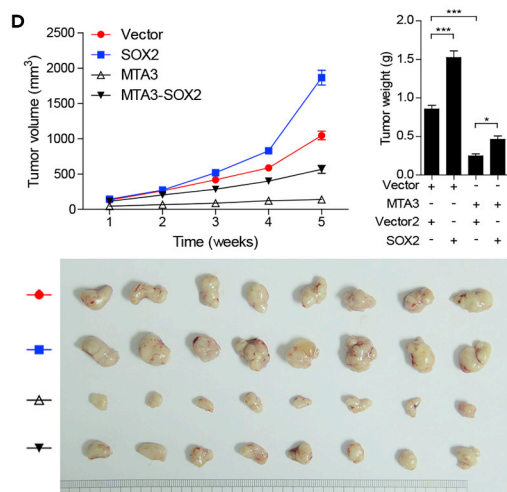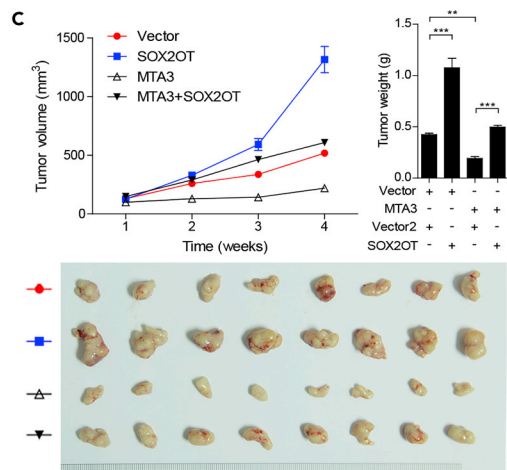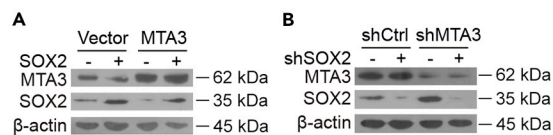
Figure 6. MTA3 Suppresses Tumor Growth via the SOX2OT-SOX2 Axis in ESCC Cells

(A and B) Western blot for MTA3 and SOX2 in EC9706 cells stably expressing MTA3 and SOX2 expression construct (A), or shMTA3 and shSOX2 construct (B). β-Actin is shown as a loading control.

(C–E) Growth curves of tumor formation of the EC9706 cells stably expressing MTA3 and SOX2OT (C) or SOX2 (D), or shMTA3 and shSOX2 (E) (upper left panel). Weight (upper right panel) and tumors (lower panel) at the end of the experiments (n = 10 per group).

(F–H) EMT and stemness markers in tumors derived from mice models injected with EC9706 cells stably expressing MTA3 and SOX2OT (F) or SOX2 (G), or shMTA3 and shSOX2 (H) detected by IHC. Scale bars: 400 μm in (F–G).

(I–K) SP$^+$ and CD44$^+$ cells in tumors derived from mice models injected with EC9706 cells stably expressing MTA3 and SOX2OT (I) or SOX2 (J), or shMTA3 and shSOX2 (K). Histograms showing the proportion of CD44$^+$ cells in the indicated cells (right panels).

Data are shown as the means of three independent experiments or representative data. Error bars indicate SEM. *$p < 0.05$, **$p < 0.01$, ***$p < 0.001$ by one-way ANOVA with post hoc intergroup comparisons.

of MTA3 lead to upregulation of both SOX2OT and SOX2, which ultimately enhances cancer stemness in ESCC.

It has been reported that GATA3 plays an important role in the regulation of CSC activities (Yang et al., 2017) and loss of GATA3 contributes to breast cancer metastasis (Si et al., 2015). In addition, GATA3 is mutated in >10% of breast tumors (The Cancer Genome Atlas Network, 2012). Mutations in the second zinc finger domain of GATA3 diminishes or abolishes its DNA-binding ability and reduces its stability in human breast cancers (Usary et al., 2004). These findings altogether suggest that GATA3 mutations are "drivers" of breast cancer development. Of note, MTA3 physically interacts with GATA3 and regulates a subset of genes that control EMT in breast cancer cells (Si et al., 2015). In this study, we identified a critical role of GATA3 in mediating MTA3-repressed SOX2OT. Of note, genetic changes (mutation, amplification, and deletion) of GATA3 are extremely rare in esophageal cancer (0.62%, Table S3). Therefore, dysfunctional MTA3, not GATA3, likely to be a "driver" in esophageal cancer development and the MTA3/SOX2OT/SOX2 axis, plays an inhibitive role in esophageal cancer stemness.

Given that MTA3 is one of the master regulators of EMT, it is not surprising to find that hundreds of genes were up- or down-regulated by MTA3 (Figure S6A). However, we conclude that SOX2, through the SOX2OT/SOX2 axis, plays an overwhelmingly prominent role in MTA3-regulated cancer stemness based on the following evidence. (1) SOX2 is the only MTA3 target among the stemness-related genes tested (Figures S6A and S6C–S6E). (2) Results from the experiments using animal models showed that MTA3 and SOX2OT and/or SOX2 are capable of inhibiting and enhancing tumor growth, respectively. More importantly, the inhibitory effect of MTA3 on tumor growth is SOX2 and SOX2OT dependent (Figure 6). (3) Both SOX2 and SOX2OT play indispensable roles in MTA3-regulated cancer stemness (Figures 4 and S8). (4) The inverse relationship between MTA3 and SOX2 is not only frequently observed in ESCC tissue but also highly correlated with patients' overall survival (Figure 5). Therefore, targeting the MTA3/SOX2OT/SOX2 axis could be an efficacious therapy for the ESCC caused by dysregulation of this axis. In fact, targeting lncRNAs *in vivo* specifically by RNA-targeting therapeutics and LNA appears to be a practically attractive clinical tool (Leucci et al., 2016). Therefore, the current study not only identified a previously unrecognized molecular mechanism in MTA3-regulated cancer stemness but also implicated a great potential of the MTA3/SOX2OT/SOX2 axis in diagnosis, prognosis, and treatment of ESCC.

Limitations of the Study

Based on the results mainly derived from overexpression and/or knockdown of different genes in cultured cells and xenograft mouse models, we were able to demonstrate that, by targeting/repressing the SOX2OT/SOX2 axis, MTA3 can suppress cancer stemness and EMT in ESCC. However, the conclusions would be strengthened if the relevant experiments were conducted in tissue-specific MTA3 transgenic and/or MTA3 knockout mice. However, owing to the lack of esophagus-specific loxP-Cre constructs currently, we will not be able to conduct such animal experiments. Furthermore, the clinical significance of this MTA3-SOX2OT/SOX2 axis needs to be validated in larger clinical cohorts (Wang et al., 2013) (Dong et al., 2017a, 2017b).

METHODS

All methods can be found in the accompanying Transparent Methods supplemental file.

iScience

CellPress

AUTHOR CONTRIBUTIONS

H.Z. and F.Z. conceived and designed the experiments; J.G. and L.D. performed bioinformatics analyses; L.W., J.G., J.L., and W.L. performed the *in vitro* experiments; L.D., L.W., and Z.Y. performed the *in vivo* experiments; J.G., L.D., and Z.Y. performed and guided the statistical analysis; Y.G., L.D., Z.Y., and Y.C. provided or collected the study materials or patients; H.Z., D.Z., R.P.C., S.-C.J.Y., and L.D. wrote the manuscript. All the authors read and approved the final manuscript.

DECLARATION OF INTERESTS

The authors have declared that no conflict of interest exists.

REFERENCES

Askarian-Amiri, M.E., Seyfoddin, V., Smart, C.E., Wang, J., Kim, J.E., Hansji, H., Baguley, B.C., Finlay, G.J., and Leung, E.Y. (2014). Emerging role of long non-coding RNA SOX2OT in SOX2 regulation in breast cancer. PLoS One 9, e102140.

Bass, A.J., Watanabe, H., Mermel, C.H., Yu, S., Perner, S., Verhaak, R.G., Kim, S.Y., Wardwell, L., Tamayo, P., Gat-Viks, I., et al. (2009). SOX2 is an amplified lineage-survival oncogene in lung and esophageal squamous cell carcinomas. Nat. Genet. 41, 1238–1242.

Bhan, A., Soleimani, M., and Mandal, S.S. (2017). Long noncoding RNA and cancer: a new paradigm. Cancer Res. 77, 3965–3981.

Bowen, N.J., Fujita, N., Kajita, M., and Wade, P.A. (2004). Mi-2/NuRD: multiple complexes for many purposes. Biochim. Biophys. Acta 1677, 52–57.

Brennan, K., Koenig, J.L., Gentles, A.J., Sunwoo, J.B., and Gevaert, O. (2017). Identification of an atypical etiological head and neck squamous carcinoma subtype featuring the CpG island methylator phenotype. EBioMedicine 17, 223–236.

Bruning, A., Juckstock, J., Blankenstein, T., Makovitzky, J., Kunze, S., and Mylonas, I. (2010). The metastasis-associated gene MTA3 is downregulated in advanced endometrioid adenocarcinomas. Histol. Histopathol 25, 1447–1456.

Chen, X., Ying, Z., Lin, X., Lin, H., Wu, J., Li, M., and Song, L. (2013). Acylglycerol kinase augments

JAK2/STAT3 signaling in esophageal squamous cells. J. Clin. Invest 123, 2576–2589.

Deshmukh, A., Binju, M., Arfuso, F., Newsholme, P., and Dharmarajan, A. (2017). Role of epigenetic modulation in cancer stem cell fate. Int. J. Biochem. Cell Biol. 90, 9–16.

Dong, H., Guo, H., Xie, L., Wang, G., Zhong, X., Khoury, T., Tan, D., and Zhang, H. (2013). The metastasis-associated gene MTA3, a component of the Mi-2/NuRD transcriptional repression complex, predicts prognosis of gastroesophageal junction adenocarcinoma. PLoS One 8, e62986.

Dong, H., Ma, L., Gan, J., Lin, W., Chen, C., Yao, Z., Du, L., Zheng, L., Ke, C., Huang, X., et al. (2017a). PTPRO represses ERBB2-driven breast oncogenesis by dephosphorylation and endosomal internalization of ERBB2. Oncogene 36, 410–422.

Dong, H., Xu, J., Li, W., Gan, J., Lin, W., Ke, J., Jiang, J., Du, L., Chen, Y., Zhong, X., et al. (2017b). Reciprocal androgen receptor/interleukin-6 crosstalk drives oesophageal carcinoma progression and contributes to patient prognosis. J. Pathol. 241, 448–462.

Feng, Y., Ke, C., Tang, Q., Dong, H., Zheng, X., Lin, W., Ke, J., Huang, J., Yeung, S.C., and Zhang, H. (2014). Metformin promotes autophagy and apoptosis in esophageal squamous cell carcinoma by downregulating Stat3 signaling. Cell Death Dis. 5, e1088.

Fujita, N., Jaye, D.L., Kajita, M., Geigerman, C., Moreno, C.S., and Wade, P.A. (2003). MTA3, a Mi-2/NuRD complex subunit, regulates an invasive growth pathway in breast cancer. Cell 113, 207–219.

Hou, Z., Zhao, W., Zhou, J., Shen, L., Zhan, P., Xu, C., Chang, C., Bi, H., Zou, J., Yao, X., et al. (2014). A long noncoding RNA Sox2ot regulates lung cancer cell proliferation and is a prognostic indicator of poor survival. Int. J. Biochem. Cell Biol. 53, 380–388.

Kumagai, Y., Tachikawa, T., Higashi, M., Sobajima, J., Takahashi, A., Amano, K., Fukuchi, M., Ishibashi, K., Mochiki, E., Yakabi, K., et al. (2018). Vascular endothelial growth factors C and D and lymphangiogenesis at the early stage of esophageal squamous cell carcinoma progression. Dis. Esophagus 31, https://doi.org/10.1093/dote/doy011.

Kumar, R., and Wang, R.A. (2016). Structure, expression and functions of MTA genes. Gene 582, 112–121.

Leone, S., and Santoro, R. (2016). Challenges in the analysis of long noncoding RNA functionality. FEBS Lett. 590, 2342–2353.

Leucci, E., Vendramin, R., Spinazzi, M., Laurette, P., Fiers, M., Wouters, J., Radaelli, E., Eyckerman, S., Leonelli, C., Vanderheyden, K., et al. (2016). Melanoma addiction to the long non-coding RNA SAMMSON. Nature 531, 518–522.

Li, H., Sun, L., Xu, Y., Li, Z., Luo, W., Tang, Z., Qiu, X., and Wang, E. (2013). Overexpression of MTA3

correlates with tumor progression in non-small cell lung cancer. PLoS One 8, e66679.

Li, X., Jia, S., Wang, S., Wang, Y., and Meng, A. (2009). Mta3-NuRD complex is a master regulator for initiation of primitive hematopoiesis in vertebrate embryos. Blood 114, 5464–5472.

Li, Z., Jiang, P., Li, J., Peng, M., Zhao, X., Zhang, X., Chen, K., Zhang, Y., Liu, H., Gan, L., et al. (2018). Tumor-derived exosomal lnc-Sox2ot promotes EMT and stemness by acting as a ceRNA in pancreatic ductal adenocarcinoma. Oncogene 37, 3822–3838.

Liau, B.B., Sievers, C., Donohue, L.K., Gillespie, S.M., Flavahan, W.A., Miller, T.E., Venteicher, A.S., Hebert, C.H., Carey, C.D., Rodig, S.J., et al. (2017). Adaptive chromatin remodeling drives glioblastoma stem cell plasticity and drug tolerance. Cell Stem Cell 20, 233–246 e237.

Manavathi, B., Singh, K., and Kumar, R. (2007). MTA family of coregulators in nuclear receptor biology and pathology. Nucl. Recept. Signal. 5, e010.

Mylonas, I., and Bruning, A. (2012). The metastasis-associated gene MTA3 is an independent prognostic parameter in uterine non-endometrioid carcinomas. Histopathology 60, 665–670.

Nassar, D., and Blanpain, C. (2016). Cancer stem cells: basic concepts and therapeutic implications. Annu. Rev. Pathol. 11, 47–76.

Ning, Z., Gan, J., Chen, C., Zhang, D., and Zhang, H. (2014). Molecular functions and significance of the MTA family in hormone-independent cancer. Cancer Metastasis Rev. 33, 901–919.

Schmitt, A.M., and Chang, H.Y. (2016). Long noncoding RNAs in cancer pathways. Cancer Cell 29, 452–463.

Shafiee, M., Aleyasin, S.A., Vasei, M., Semnani, S.S., and Mowla, S.J. (2016). Down-regulatory effects of miR-211 on long non-coding RNA SOX2OT and SOX2 genes in esophageal squamous cell carcinoma. Cell J. 17, 593–600.

Shahryari, A., Rafiee, M.R., Fouani, Y., Oliae, N.A., Samaei, N.M., Shafiee, M., Semnani, S., Vasei, M., and Mowla, S.J. (2014). Two novel splice variants of SOX2OT, SOX2OT-S1, and SOX2OT-S2 are coupregulated with SOX2 and OCT4 in esophageal squamous cell carcinoma. Stem Cells 32, 126–134.

Shan, S., Hui, G., Hou, F., Shi, H., Zhou, G., Yan, H., Wang, L., and Liu, J. (2015). Expression of metastasis-associated protein 3 in human brain glioma related to tumor prognosis. Neurol. Sci. 36, 1799–1804.

Si, W., Huang, W., Zheng, Y., Yang, Y., Liu, X., Shan, L., Zhou, X., Wang, Y., Su, D., Gao, J., et al. (2015). Dysfunction of the reciprocal feedback loop between GATA3- and ZEB2-nucleated repression programs contributes to breast cancer metastasis. Cancer Cell 27, 822–836.

The Cancer Genome Atlas Network. (2012). Comprehensive molecular portraits of human breast tumours. Nature 490, 61–70.

Toh, Y., and Nicolson, G.L. (2009). The role of the MTA family and their encoded proteins in human cancers: molecular functions and clinical implications. Clin. Exp. Metastasis 26, 215–227.

Tosetti, V., Sassone, J., Ferri, A.L.M., Taiana, M., Bedini, G., Nava, S., Brenna, G., Di Resta, C., Pareyson, D., Di Giulio, A.M., et al. (2017). Transcriptional role of androgen receptor in the expression of long non-coding RNA Sox2OT in neurogenesis. PLoS One 12, e0180579.

Usary, J., Llaca, V., Karaca, G., Presswala, S., Karaca, M., He, X., Langerod, A., Karesen, R., Oh, D.S., Dressler, L.G., et al. (2004). Mutation of

GATA3 in human breast tumors. Oncogene 23, 7669–7678.

Visvader, J.E., and Lindeman, G.J. (2012). Cancer stem cells: current status and evolving complexities. Cell Stem Cell 10, 717–728.

Wang, P., Shan, L., Xue, L., Zheng, B., Ying, J., and Lu, N. (2017). Genome wide copy number analyses of superficial esophageal squamous cell carcinoma with and without metastasis. Oncotarget 8, 5069–5080.

Wang, Q., Ma, C., and Kemmner, W. (2013). Wdr66 is a novel marker for risk stratification and involved in epithelial-mesenchymal transition of esophageal squamous cell carcinoma. BMC Cancer 13, 137.

Yang, Z., He, L., Lin, K., Zhang, Y., Deng, A., Liang, Y., Li, C., and Wen, T. (2017). The KMT1A-GATA3-STAT3 circuit is a novel self-renewal signaling of human bladder cancer stem cells. Clin. Cancer Res. 23, 6673–6685.

Yao, Y.L., and Yang, W.M. (2003). The metastasis-associated proteins 1 and 2 form distinct protein complexes with histone deacetylase activity. J. Biol. Chem. 278, 42560–42568.

Zhang, H., Singh, R.R., Talukder, A.H., and Kumar, R. (2006a). Metastatic tumor antigen 3 is a direct corepressor of the Wnt4 pathway. Genes Dev. 20, 2943–2948.

Zhang, H., Stephens, L.C., and Kumar, R. (2006b). Metastasis tumor antigen family proteins during breast cancer progression and metastasis in a reliable mouse model for human breast cancer. Clin. Cancer Res. 12, 1479–1486.

Zhang, J.J., Zhu, Y., Zhang, X.F., Liu, D.F., Wang, Y., Yang, C., Shi, G.D., Peng, Y.P., Zhang, K., Tian, L., et al. (2017). Yin Yang-1 suppresses pancreatic ductal adenocarcinoma cell proliferation and tumor growth by regulating SOX2OT-SOX2 axis. Cancer Lett. 408, 144–154.

Supplemental Information

MTA3 Represses Cancer Stemness

by Targeting the SOX2OT/SOX2 Axis

Liang Du, Lu Wang, Jinfeng Gan, Zhimeng Yao, Wan Lin, Junkuo Li, Yi Guo, Yuping Chen, Fuyou Zhou, Sai-Ching Jim Yeung, Robert P. Coppes, Dianzheng Zhang, and Hao Zhang

Supplemental figures and legends
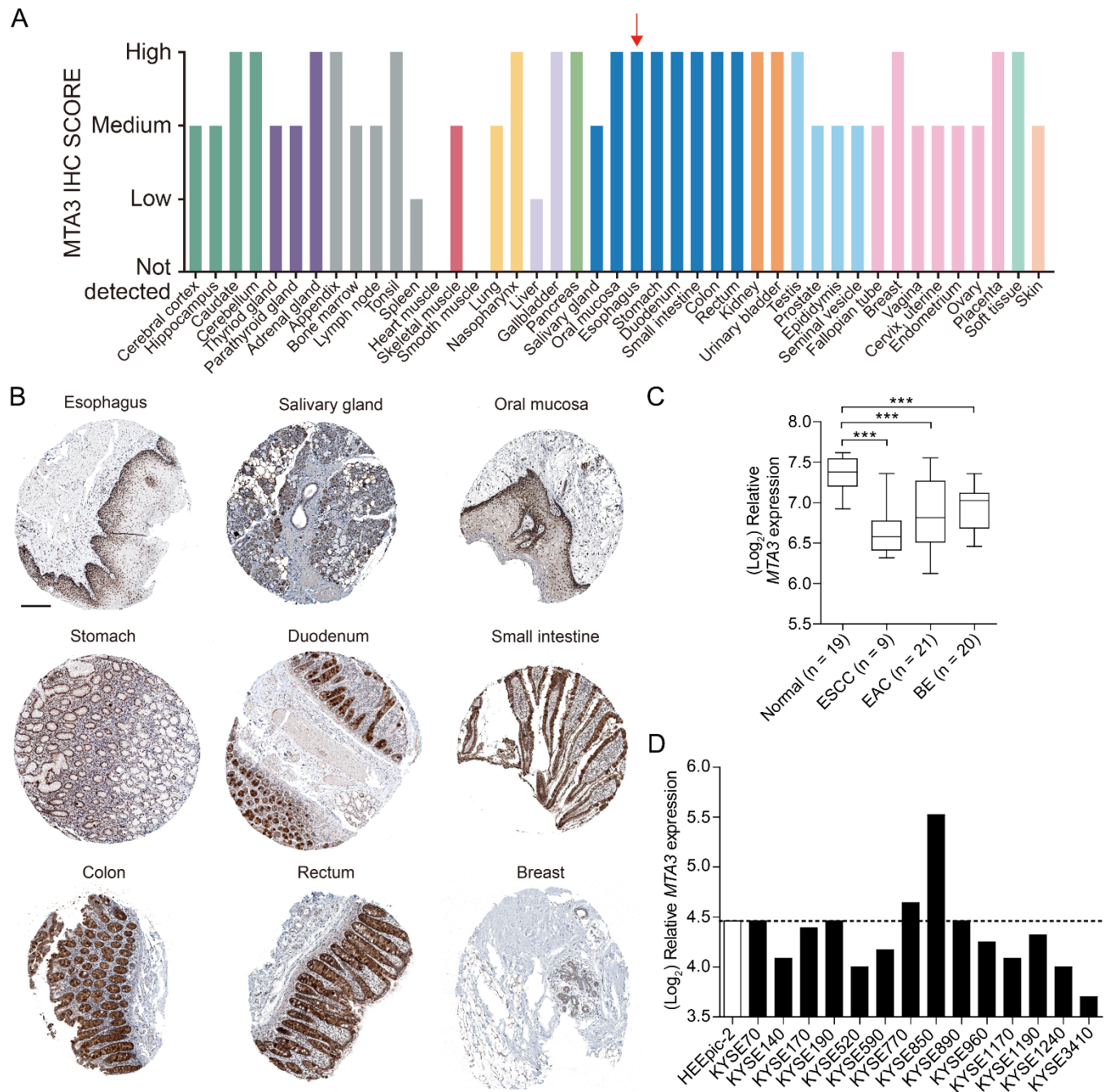
Figure S1. Related to Figure 1. MTA3 is highly enriched in human digestive organs and downregulated in human esophageal squamous cell carcinoma (ESCC). (A) IHC score of MTA3 in various human normal organs was investigated in the Human Protein Atlas database, red arrow indicates *esophagus*. (B) Representative IHC images of MTA3 in the indicated digestive organs, including esophagus, breast was used as positive control. All images were obtained from Human Protein Atlas database. Scale bars: 200 μm. (C) *MTA3* mRNA expression in an ESCC microarray dataset from GEO, GSE26886. (D)

MTA3 mRNA expression in a panel of ESCC cell lines (filled bars) and normal esophageal epithelium cells (open bar) was analyzed in a microarray dataset from GEO, GSE23964. ***p< 0.001 by one-way ANOVA with post hoc intergroup comparisons.

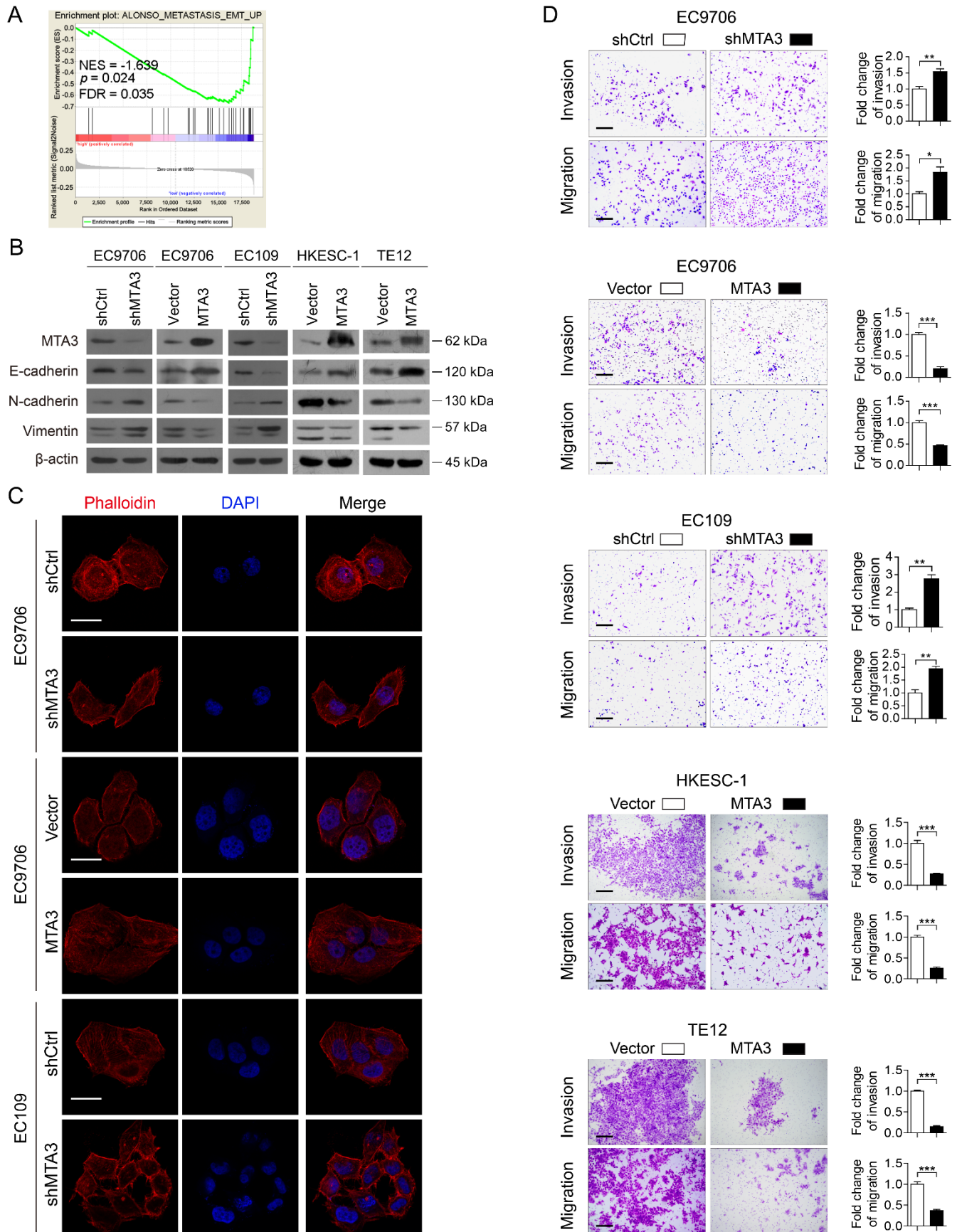**Figure S2. Related to Figure 2. MTA3 suppresses the metastatic potential of ESCC cells *in vitro*. (A)** GSEA plots of enrichment of ALONSO_METASTASIS_EMT_UP signatures in MTA3[High] tumors versus MTA3[Low] tumors in GSE23400 dataset. **(B)** Western blot of the indicated epithelial or mesenchymal

markers and MTA3 in EC9706 cells with MTA3 depletion or overexpression, and EC109 cells with MTA3 depletion, and in HKESC-1 cells and TE12 cells with MTA3 overexpression. β-actin is shown as a loading control. (**C**) Representative images of phalloidin staining of EC9706 cells with MTA3 depletion or overexpression and EC109 cells with MTA3 depletion. Scale bars: 20 μm. (**D**) Invasion or migration of EC9706 cells with MTA3 depletion or overexpression, EC109 cells with MTA3 depletion, and HKESC-1 cells and TE12 cells with MTA3 overexpression were measured by transwell assay with or without matrigel. Scale bars: 200 μm. Data were shown as means of three independent experiments. Error bars indicate SEM. *$p < 0.05$, **$p < 0.01$, ***$p < 0.001$ by Student's t-test.
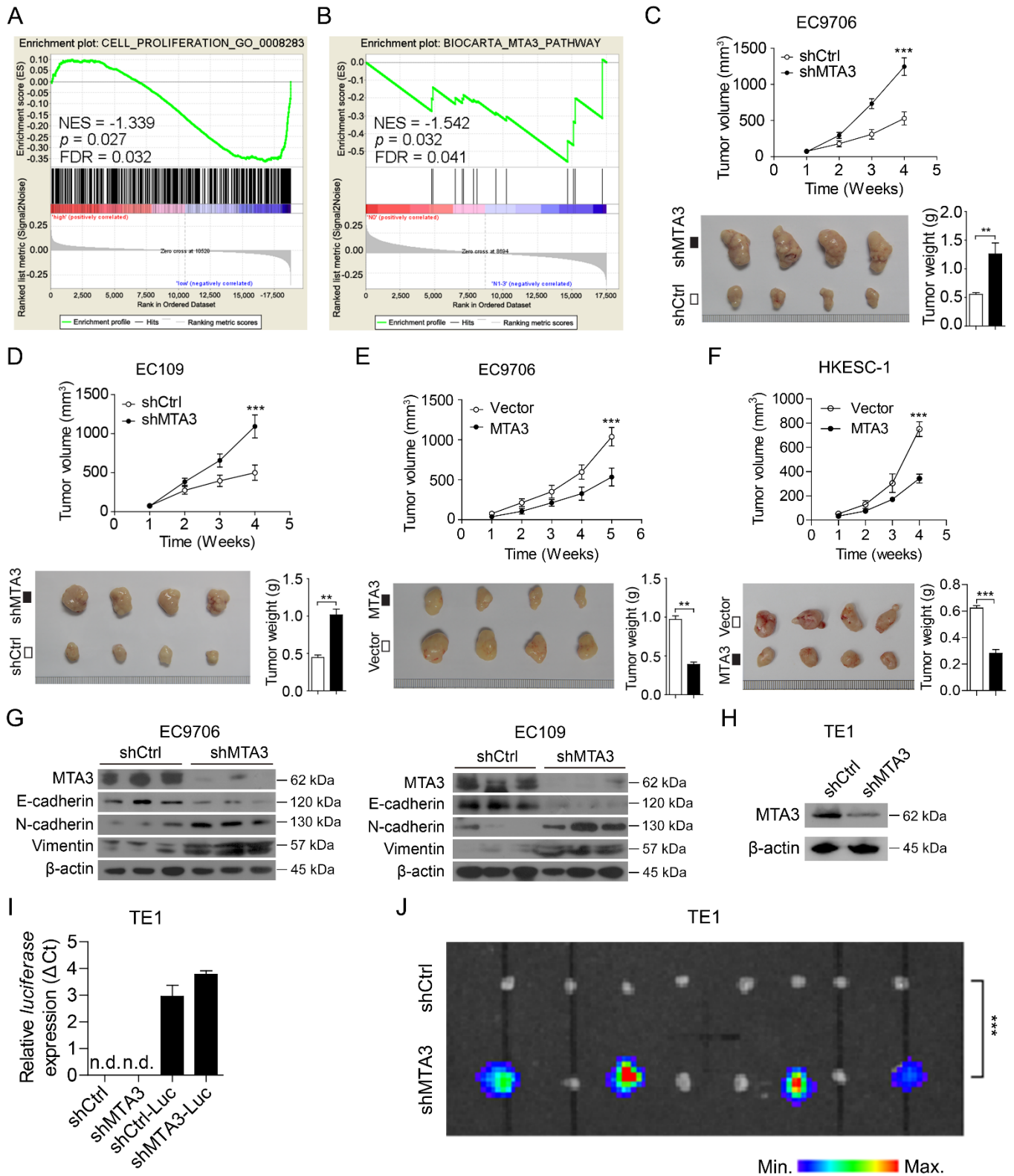
Figure S3. Related to Figure 2. MTA3 regulates the tumor growth of ESCC cells and metastasis *in vivo*. (**A**) GSEA plots of enrichment of CELL_PROLIFERATION_GO_0008283 signatures in MTA3[High] tumors versus MTA3[Low] tumors in the GSE23400 dataset. (**B**) GSEA plots of enrichment of BIOCARTA_MTA3_PATHWAY in ESCC tissues with non-lymph node metastasis versus ESCC tissues with lymph node metastasis in the GSE47404 dataset. (**C**) Growth curves for tumor formation of the

EC9706 cells with MTA3 depleted were generated (upper panel). Tumors were resected (lower left panel) and weighed (lower right panel) at the end of the experiments (n = 5 shCtrl, n = 5 shMTA3). (**D**) Growth curves for tumor formation of the EC109 cells MTA3 depleted were generated (upper panel). Tumors were resected (lower left panel) and weighed (lower right panel) at the end of the experiments (n = 5 shCtrl, n = 5 shMTA3). (**E**) Growth curves for tumor formation of the EC9706 cells with MTA3 overexpressed were generated (upper panel). Tumors were resected (lower left panel) and weighed (lower right panel) at the end of the experiments (n = 5 Vector, n = 5 MTA3). (**F**) Growth curves for tumor formation of the HKESC-1 cells with MTA3 overexpressed were generated (upper panel). Tumors were resected (lower left panel) and weighed (lower right panel) at the end of the experiments (n = 5 Vector, n = 5 MTA3). (**G**) Western blot of the indicated epithelial or mesenchymal markers and MTA3 in tumors derived from EC9706 cells with MTA3 depleted (left panel) and EC109 cells with MTA3 depleted (right panel). (**H**) Western blot of MTA3 in TE1 cells with MTA3 depleted. (**I**) TE1 cells that transfected with shMTA3 or shCtrl were infected with lentiviruses carrying luciferase and then subjected for RNA extraction followed by qRT-PCR analysis of luciferase gene. (**J**) The TE1 cells with or without MTA3 depleted were infected with recombinant lentiviruses carrying luciferase and injected subcutaneously into the flanks of nude mice (n = 8). The inguinal lymph nodes of the mice were extracted and analyzed for the presence of metastatic cells by bioluminescence imaging. Data were shown as the means from at least three independent experiments or representative data. Error bars indicate SEM. **$p<0.01$, ***$p<0.001$ by Student's t-test or chi-square test, where appropriate.
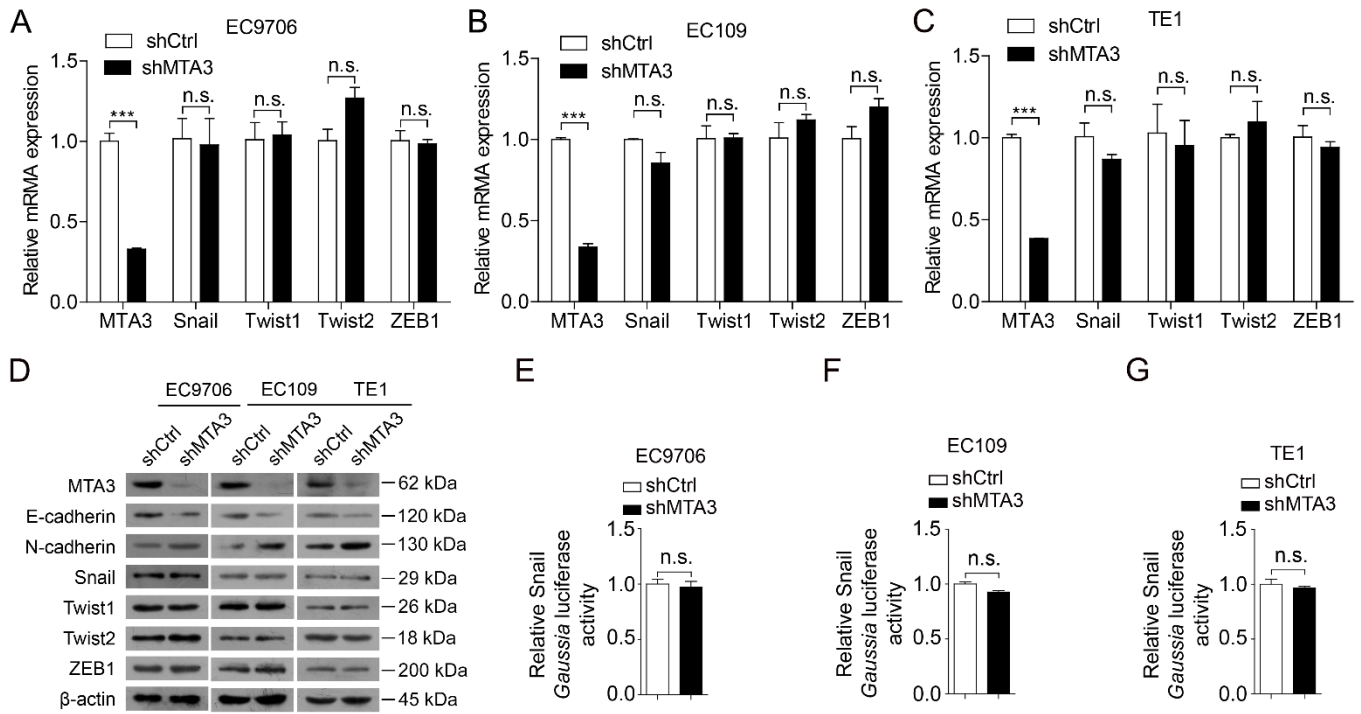
Figure S4. Related to Figure 2. MTA3 shows no effect on canonical EMT regulators. (**A-C**) QRT-PCR of *MTA3*, *Snai1*, *Twist1*, *Twist2* and *ZEB1* in EC9706 (A), EC109 (B) and TE1 (C) cells with MTA3 depleted. (**D**) Western blot of the indicated epithelial and mesenchymal markers, or EMT regulators in the indicated cells. (**E-G**) Snai1 luciferase reporter activity was analyzed in EC9706 (E), EC109 (F) and TE1 (G) cells with MTA3 depleted. Data were shown as the means from at least three independent experiments or representative data. Error bars indicate SEM. n.s., not statistically significant; ***$p<0.001$ by Student's *t*-test.
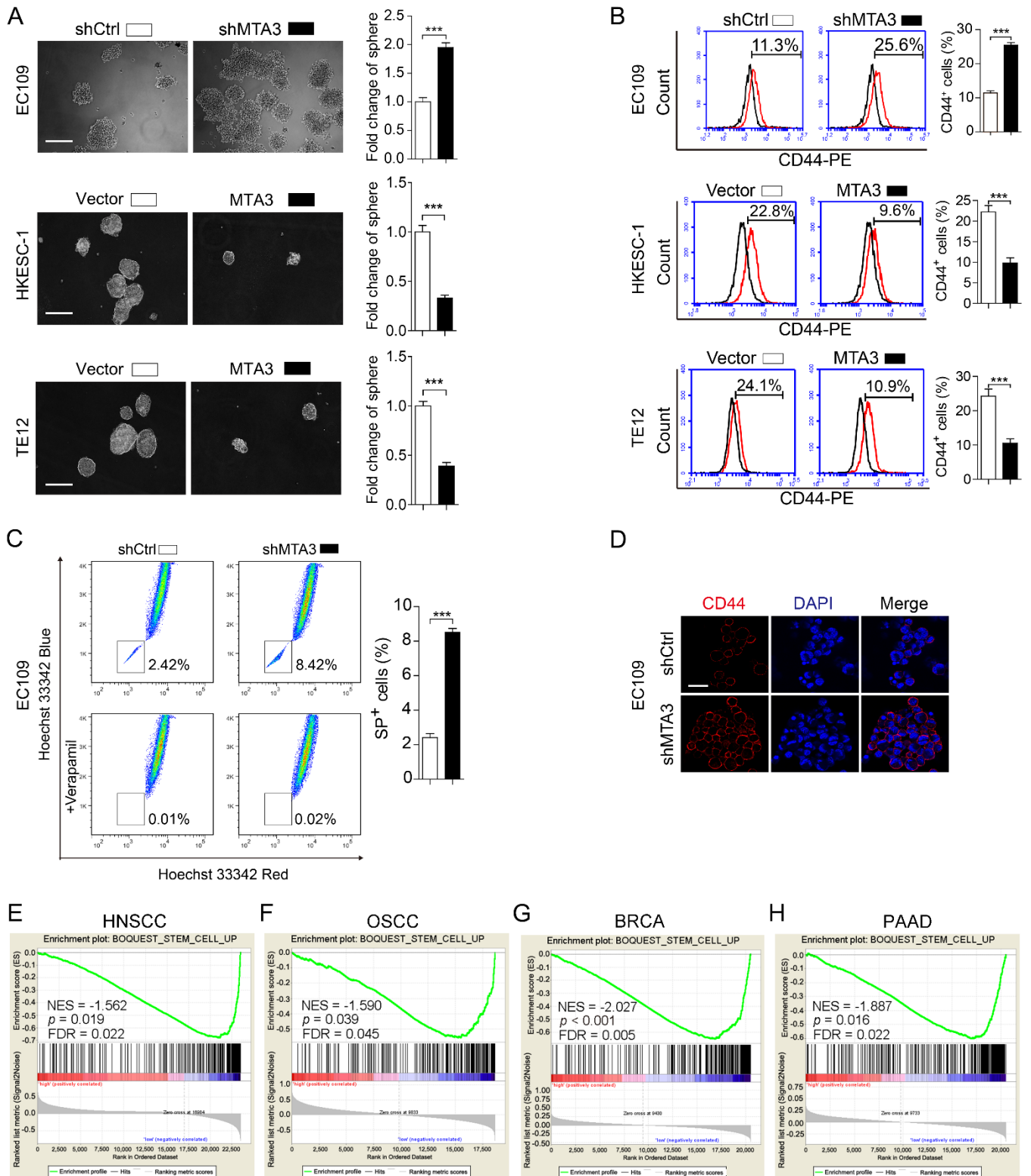
Figure S5. Related to Figure 2. MTA3 regulates stemness in ESCC cells and negatively correlates with stemness signature in various cancers. (**A**) Representative images of spheres formed by EC109 cells with MTA3 depleted, or HKESC-1 cells and TE12 cells with MTA3 overexpressed (left panel). Histograms showing the fold change in the number of spheres formed by EC109 cells with MTA3 depleted (right panel). Scale bars: 200 μm. (**B**) Flow cytometry analysis of the CD44$^+$ population in EC109 cells with MTA3

depleted, or HKESC-1 cells and TE12 cells with MTA3 overexpressed. Histograms showing the proportion of CD44$^+$ cells in the indicated cells (right panel). (**C**) Hoechst 33342 dye exclusion assay of the SP$^+$ population in EC109 cells with MTA3 depleted. Histograms showing the proportion of SP$^+$ cells in EC109 cells with MTA3 depleted (right panel) (**D**) Representative images of immunofluorescence for CD44 expression in EC109 cells with MTA3 depleted. Scale bars: 40 μm. (**E-H**) GSEA plots of enrichment of BOQOEST_STEM_CELL_UP signatures in MTA3^{High} tumors versus MTA3^{Low} tumors in the HNSCC (GEO dataset GSE10300, n = 44), OSCC (GEO dataset GSE37991, n = 40), BRCA (TCGA dataset, n = 1222), PAAD (TCGA dataset, n = 182). Data were shown as the means from at least three independent experiments or representative data. Error bars indicate SEM. ***$p<0.001$ by Student's *t*-test.
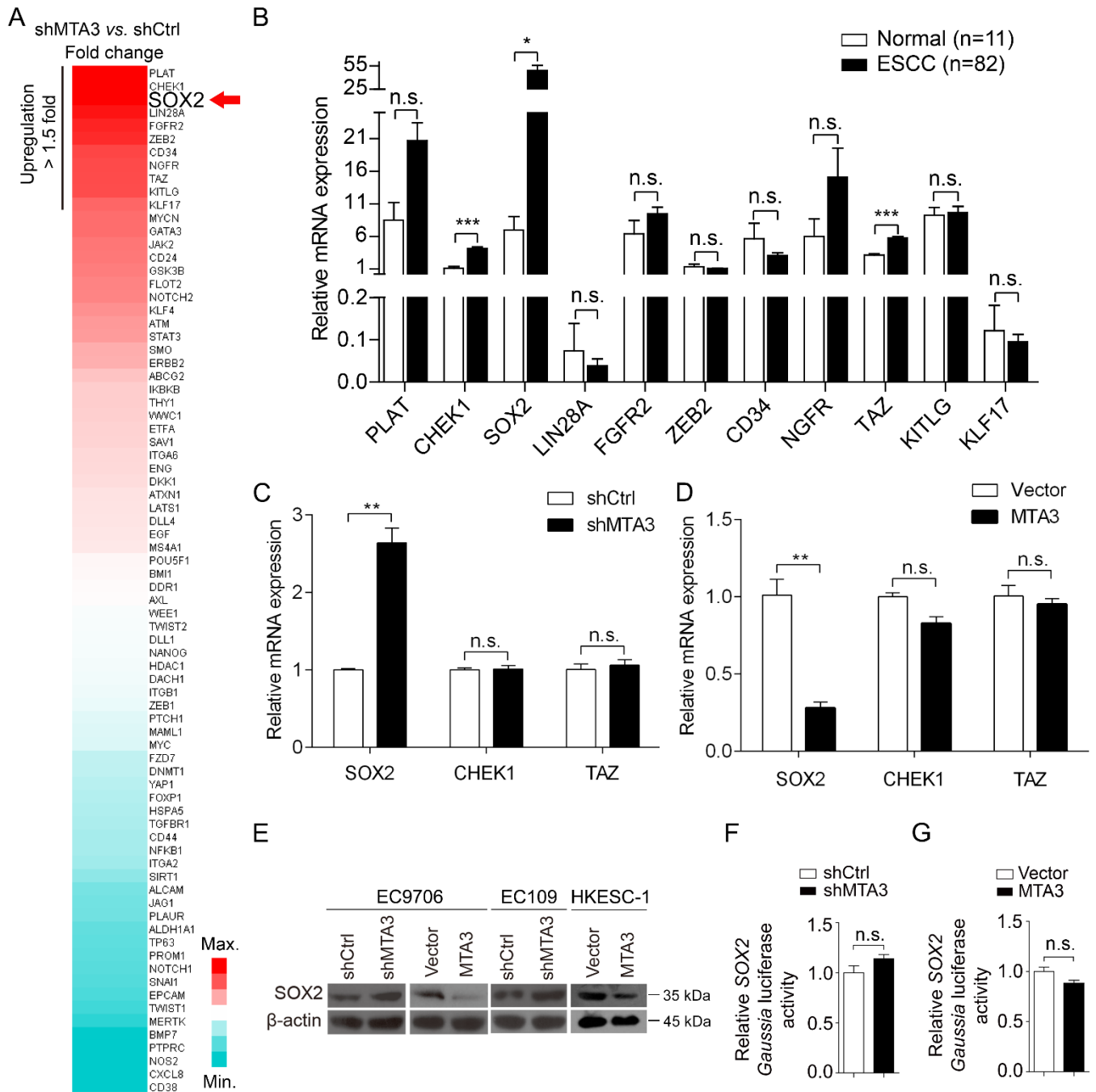
Figure S6. Related to Figure 3. MTA3 suppresses SOX2 expression indirectly. (**A**) Heat map showing fold change expression of stemness signatures in shMTA3 versus shCtrl EC9706 cells based on qPCR array. (**B**) The expression of 11 genes upregulated by MTA3 depletion (more than 1.5 folds) was analyzed in ESCC using TCGA dataset (Titled ESCA), which includes 82 ESCC tissues and 11 normal esophageal tissues. (**C** and **D**) QRT-PCR of SOX2, CHEK1, and TAZ in the indicated cells with MTA3 depleted (C) or overexpressed (D). (**E**) Western blot of SOX2 in EC9706 cells with MTA3 depleted or overexpressed and EC109 cells with MTA3 depleted, and HKECS-1 with MTA3 overexpressed. (**F and G**) SOX2 luciferase

reporter was transfected into EC9706 cells with MTA3 depleted (F) or overexpressed (G). The relative SOX2 Gaussia luciferase reporter activities were measured at 72 h after transfection. Data were shown as the means from at least three independent experiments or representative data. Error bars indicate Error bars indicate SEM. n.s., not statistically significant, *$p<0.05$, **$p<0.01$, **$p<0.01$ by Student's *t*-test.
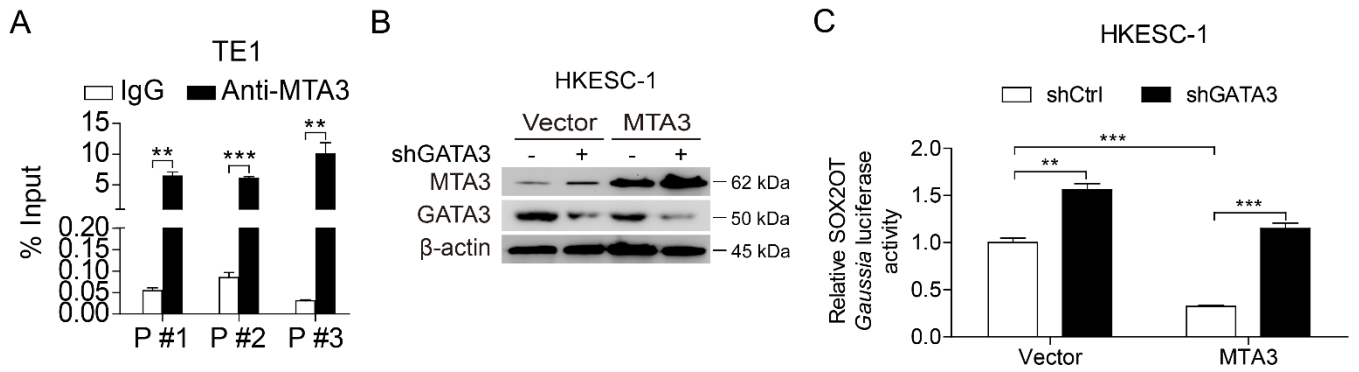
Figure S7. Related to Figure 3. MTA3-repressed SOX2OT transcription depends on GATA3. (**A**) ChIP assay using antibodies against MTA3 or IgG. qPCR to detect the enriched DNA fragments in the SOX2OT promoter region in TE1 cells. (**B**) Western blot of GATA3 in HKESC-1 transfected with the MTA3 or shGATA3 plasmids or in combinations between MTA3 and shGATA3. β-actin is shown as a loading control. (**C**) SOX2OT luciferase reporter activity in MTA3 overexpressed HKESC-1 cells that transfected with shGATA3 expressing plasmid. Data were shown as the means of three independent experiments or representative data. Error bars indicate SEM. **$p < 0.01$, ***$p < 0.001$ by Student's t-test or a one-way ANOVA with post hoc intergroup comparisons, where appropriate.
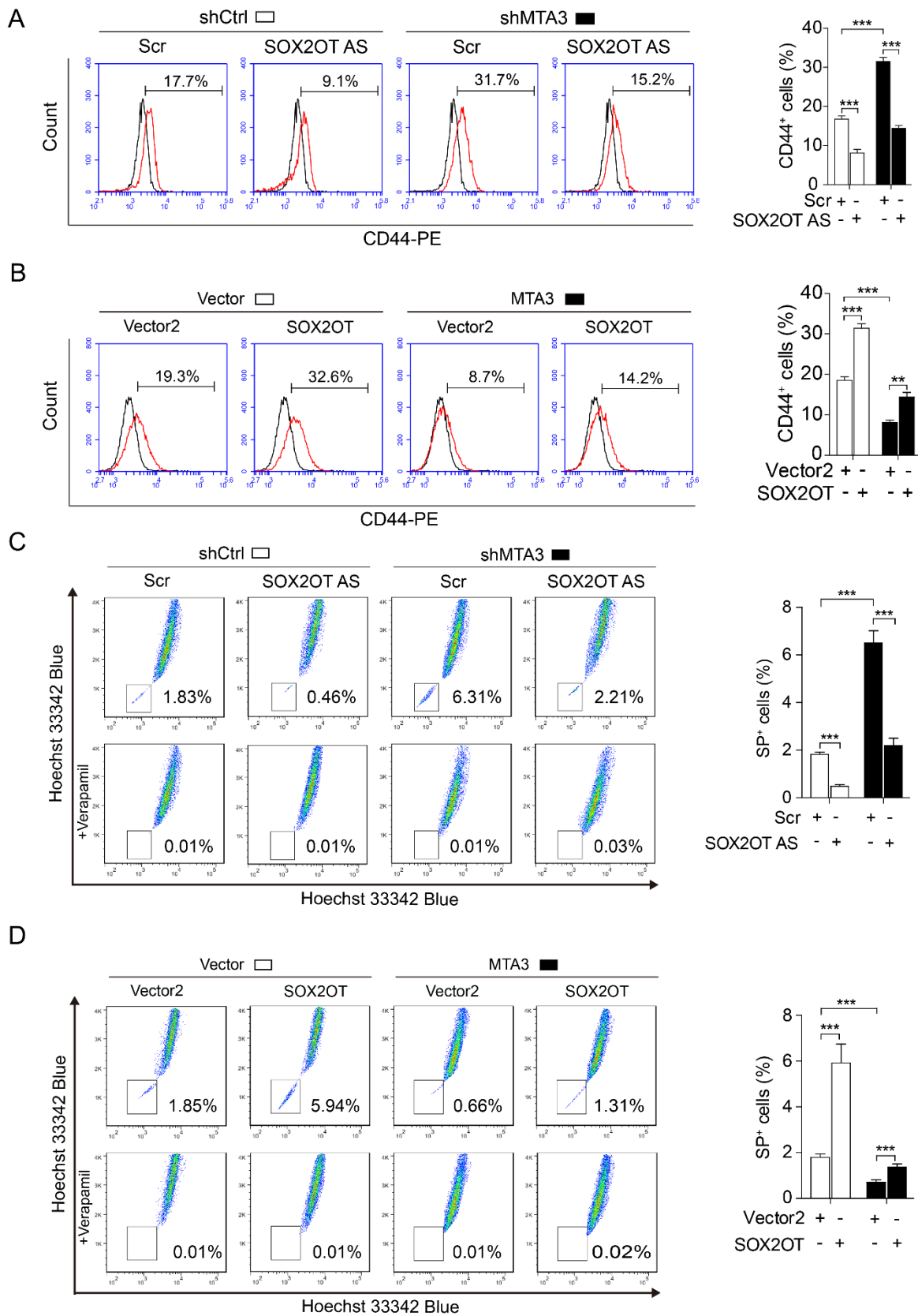
Figure S8. Related to Figure 4. MTA3 regulates CD44$^+$ population and SP$^+$ population via SOX2OT.

(**A** and **B**) EC9706 cells transfected with a combination of the shMTA3 expressing plasmid and SOX2OT

AS oligo (A), or of the MTA3 and SOX2OT expressing plasmid (B) were subjected to flow cytometry

analysis of the CD44$^+$ population. (**C** and **D**) EC9706 cells transfected with a combination of the shMTA3 expressing plasmid and SOX2OT AS oligo (C), or of the MTA3 and SOX2OT expressing plasmid (D) were subjected to Hoechst 33342 dye exclusion assay of the SP$^+$ population. Histograms showing the positive formed by the indicated cells (right panels). Data were shown as the means from at least three independent experiments or representative data. Error bars indicate SEM. ***p< 0.001 by one-way ANOVA with post hoc intergroup comparisons.

Supplemental tables

Table S1. Related to Figure 1. Relationship between MTA3 expression and clinicopathologic variables in tissue samples of ESCC

Variables	No. of patients	MTA3 expression		p-value
		Low, no. (%)	High, no. (%)	
All patients	125	78 (62.4)	47 (37.6)	
Gender				
Male	93	58 (62.4)	35 (37.6)	0.989
Female	32	20 (62.5)	12 (37.5)	
Age (years)				
< 60	63	42 (66.7)	21(33.3)	0.321
≥ 60	62	36(58.1)	26 (61.9)	
Histologic grade				
Well	46	28 (60.9)	18 (39.1)	0.112
Moderate	64	37 (57.8)	27 (42.2)	
Poor	15	13 (86.7)	2 (13.3)	
Tumor size				
< 5 cm	46	31 (67.4)	15 (32.6)	0.379
≥ 5 cm	79	47 (59.5)	32 (40.5)	
Tumor depth				
T_1/T_2	23	9(39.1)	14 (60.9)	0.011
T_3/T_4	102	69 (67.6)	33 (32.4)	
Lymph node metastasis				
Negative	55	35(63.6)	20 (36.4)	0.800
Positive	70	43(61.4)	27 (38.6)	
Stage				
I-II	39	19(48.7)	20 (51.3)	0.033
III	86	59(68.6)	27 (31.4)	

[a.] ESCC, esophageal squamous cell carcinoma.

Table S2. Related to Figure 1. Univariate and multivariate Cox proportional hazards model predicting survival in ESCC

Variables	Univariate analysis HR (95% CI)	p-value	Multivariate analysis HR (95% CI)	p-value
Gender				
Male vs. Female	1.421(0.730-2.766)	0.301	1.787 (0.901-3.544)	0.097
Age				
≥ 60 *vs.* <60	1.526 (0.880-2.645)	0.132	1.712 (0.973-3.014)	0.062
Histologic grade				
Poor / Moderate *vs.* Well	1.586 (0.879-2.860)	0.126	1.663 (0.855-3.235)	0.134
Tumor size				
≥ 5 cm *vs.* < 5 cm	1.237 (0.698-2.191)	0.466	1.062 (0.586-1.922)	0.844
Tumor depth				
T_3/T_4 *vs.* T_1/T_2	3.332 (1.200-9.246)	0.021	1.487 (0.494-4.472)	0.480
Lymph node metastasis				
Positive *vs.* Negative	1.484 (0.844-2.612)	0.170	0.911 (0.465-1.783)	0.786
Stage				
III *vs.* I/II	3.940 (1.774-8.750)	0.001	3.417 (1.360-8.586)	0.009
MTA3 expression				
Low *vs.* High	2.988 (1.498-5.958)	0.002	2.717 (1.333-5.537)	0.006

[a] ESCC, esophageal squamous cell carcinoma; [b] HR, hazard ratio; [c] CI, confidence interval.

Table S3. Related to Figure 3. Summary of GATA3 genetic change in ESCC

Study cohorts	Mutation	Amplification	Deletion	Total
Esophageal Carcinoma (TCGA, Provisional)	0	1	1	96
Esophageal Squamous Cell Carcinoma (UCLA, Nat Genet 2014)	0	0	0	139
Esophageal Squamous Cell Carcinoma (ICGC, Nature 2014)	0	0	0	88
Total	0	1	1	323

[a.] ESCC, esophageal squamous cell carcinoma; [b.] TCGA, the Cancer Genome Atlas; [c.] UCLA, University of California, Los Angeles; [d.] ICGC, International Cancer Genomics Consortium.

Transparent Methods

Clinical patients and samples

Paraffin-embedded specimens and snap-frozen fresh ESCC tissues with their normal adjacent tissues were obtained from ESCC patients underwent surgeries at Affiliated Tumor Hospital of Shantou University Medical College. All samples were histopathologically and clinically diagnosed as ESCC. Patients who underwent preoperative neoadjuvant chemotherapy or radiotherapy for ESCC were excluded from this study.

Tissue microarray and immunohistochemistry

A tissue microarray (TMA) was conducted using paraffin-embedded specimens from 125 ESCC patients (male, n = 93; Female, n = 32) and their normal adjacent tissues as previously described (Dong et al., 2017b). Immunohistochemistry (IHC) staining was performed as previously described (Dong et al., 2017b). Briefly, the TMA blocks or the tumor xenograft tissues were sliced into 4-μm sections and immune-stained with antibodies against MTA3 (Bethyl Laboratories Inc., catalog no. A300-160A), SOX2 (Cell Signaling Technology, catalog no. 23064), or CD44 (Cell Signaling Technology, catalog no. 3570). Immunostaining scores were determined by combination of staining intensity and the percentage of positively stained cells. Staining intensity was categorized as follows: 1, negative; 2, light yellow; 3, brown. The proportion of positive cells was scored as follows: 0 (0% positive cells); 1 (1%–25% positive cells); 2 (26%–50% positive cells); 3 (51%–75% positive cells); 4 (76%–100% positive cells). Two independent pathologists without the clinical and pathological information independently reviewed and scored the immunostaining.

Cell lines and cell culture

The human ESCC cell lines EC109 and EC9706 (obtained from the Cell Bank of the Chinese Academy of

Sciences, Shanghai, China), and HKESC-1, HKESC-2, and HKESC-3 (kindly provided by Dr. S.W. Tsao, University of Hong Kong, China), and KYSE510 (obtained from the American Type Culture Collection) were cultured in RPMI 1640 (Gibco/Invitrogen) supplemented with 10% FBS (Gibco/Invitrogen). TE1 and TE12 (kindly provided by Dr. X.C. Xu, UT M.D. Anderson Cancer Center, USA) were cultured in Dulbecco's Modified Eagle Media (DMEM, Gibco/Invitrogen) supplemented with 10% FBS (Gibco/Invitrogen). The human immortalized esophageal epithelial cell lines NE2 and NE3 (kindly provided by Dr. S.W. Tsao, University of Hong Kong, China) were cultured in Defined Keratinocyte-SFM medium (DK-SFM, Gibco/Invitrogen). EC109, EC9706, HKEC-1, HKESC-3, TE1 and TE12 were derived from male patients with ESCC. HKESC-2 and KYSE-510 were derived from female patients with ESCC. NE2 and NE3 were derived from normal human esophageal tissue samples.

Transfection and infection

The full-length cDNA of MTA3 was PCR amplified from EC9706 cells and cloned into the pCDNA3.1-flag plasmid. The shRNA targeting human MTA3 (target sequence: GAGGATACCTTCTTCTACTCA) was cloned into pBabe/U6 plasmid. The plasmid carrying SOX2, and the plasmid carrying shGATA3 or shSOX2 targeted to the human GATA3 or SOX2 (shGATA3 target sequence: GATGCAAGTCCAGGCCCAA; shSOX2 target sequence: GGTTGACACCGTTGGTAATTT) were obtained from GeneCopoeia. The pEZX-PG04 plasmid carrying double-expression cassette for *Gaussia* luciferase (GLuc) under the control of the SOX2OT, SOX2, or Snai1 promoter, and secreted Alkaline Phosphatase (SeAP) under the control of CMV promoter were obtained from GeneCopoeia. pIRES2-ZsGreen1-SOX2OT plasmid and SOX2OT-GLuc plasmid with deletion of GATA3 binding sites between −1176 to −1169 bp (ΔGATA3 #1), −861 to −854 bp (ΔGATA3 #2), −291 to −284 bp (ΔGATA3 #3), or all the three GATA3 binding sites were constructed by Youbio (Hunan, China). The antisense locked nucleic acid (LNA) GapmeR targeting SOX2OT (SOX2OT AS): 5'-TCTTACTGAATGGAGG-3' and non-targeting LNA GapmeR (Scr): 5'-

AACACGTCTATACGC-3' were obtained from Exiqon (Vedbaek, Denmark). Recombinant lentiviruses carrying luciferase gene were obtained from GeneChem (Shanghai, China). Transfection of plasmids or LNA GapmeR was performed using Lipofectamine 3000 (Thermo Fisher Scientific, catalog no. L3000015) according to the manufacturer's instructions. Concentrated viruses carrying luciferase gene were used to infect cells in a 6-well plate with 10 μg/ml polybrene.

The quantitative real-time PCR assay

Total RNA was isolated from cultured cells, ESCC tissues or xenograft tissues by the TRIzol reagent (ThermoFisher, catalog no. 15596-018), and reverse transcribed using High Capacity cDNA Reverse Transcription Kit (Applied Biosystems, catalog no. 4368813) according to the manufacturer instructions. The cDNA was amplified and quantified in the ABI-7500 system (Applied Biosystems) by using SYBR Green Master (Roche). The cDNA was subjected to quantitative real-time PCR (qRT-PCR) with the following primers: *MTA3* forward: 5'-AAGCCTGGTGCTGTGAAT-3' and reverse: 5'-AGGGTCCTCTGTAGTTGG-3'; *SOX2OT* forward: 5'-GCTCGTGGCTTAGGAGATTG-3' and reverse: 5'-CTGGCAAAGCATGAGGAACT-3'; *SOX2* forward: 5'-CATCACCCACAGCAAATGACA-3' and reverse: 5'-GCTCCTACCGTACCACTAGAACTT-3'; *Snail* forward: 5'-TCTGAGGCCAAGGATCTCCA-3' and reverse: 5'-CATTCGGGAGAAGGTCCGAG-3'; *Twist1* forward: 5'-AGACCTAGATGTCATTGTTTCCA-3' and reverse: 5'-TTGGCACGACCTCTTGAGAAT-3'; *Twist2* forward: 5'-CTGCCATTGCCAGACCTTCT-3' and reverse: 5'-GATGGTGTTGGCAGTGTTGC-3'; *ZEB1* forward: 5'-TTCTCCCTCCCCTCTGGGAT-3' and reverse: 5'-CCTATGCTCCACTCCTTGCT-3'; *Luciferase* forward: 5'-ACTGGGACGAAGACGAACAC-3' and reverse: 5'-GGCGACGTAATCCACGATCT-3'; *β-actin* forward: 5'-GAACCCCAAGGCCAACCGCGAGA-3' and reverse: 5'-TGACCCCGTCACCGGAGTCCATC-3'.

Western blot analysis

Proteins in the lysates of the cultured cells or xenograft tissues were separated on SDS-PAGE, transferred onto the PVDF membranes. The membranes were incubated with primary antibodies against MTA3 (Bethyl Laboratories Inc., catalog no. A300-160A), SOX2 (Cell Signaling Technology, catalog no. 23064), E-Cadherin (BD Bioscience, catalog no. 610181), N-Cadherin (BD Bioscience, catalog no. 610920), Vimentin (Cell Signaling Technology, catalog no. 3932), GATA3 (Santa Cruz Biotechnology, catalog no. sc-268), Snai1 (Cell Signaling Technology, catalog no. 3879), Twist1 (Cell Signaling Technologies, catalog no. 46702), Twist2 (Abcam, catalog no. ab66031), and ZEB1 (Abcam, catalog no. ab203829), and β-actin (Cell Signaling Technology, catalog no. 4970), followed by HRP-conjugated secondary antibodies as previously described (Feng et al., 2014). Protein bands were visualized with SuperSignal West Pico Luminol/Enhancer Solution (Thermo Scientific).

Transwell assay

After starvation for 24 h, the cells (1×10^5) in 200ul serum-free RPMI 1640 were seeded onto the upper compartment of a 24-well chamber pre-coated with (Invasion assay) or without (Migration assay) matrigel (BD Biosciences, catalog no. 356234). The lower compartment was filled with 500ul RPMI 1640 supplemented with 10% FBS. After 24-48 h of incubation, the invaded/migrated cells were fixed with methanol, stained with 0.1% crystal violet, and counted under a microscope. All experiments were performed in triplicate.

Phalloidin staining

Cells were fixed with 4% paraformaldehyde for 20 min and blocked in 5% BSA for 30 min at room temperature. Fixed cells were then incubated with 5μg/ml of phalloidin (Invitrogen, catalog no. A12381) in dark for 30 min at 37°C. Phalloidin staining was observed under ZEISS LSM800 confocal fluorescence microscope (ZEISS, Germany).

Sphere formation assays

Cells were seeded in 6-well ultra-low attachment plates (Corning, catalog no. 3471) in DMEM/F12 serum-free medium (Gibco/Invitrogen) supplemented with 10 ng/ml EGF (PeproTech, catalog no. AF-100-15), 10 ng/ml bFGF (PeproTech, catalog no. 100-18B) and 1×N2 (Life Technologies, catalog no. 17502-048). After incubation of 1-2 weeks, the number of tumorspheres was counted under a microscope (Olympus, Tokyo, Japan).

Flow cytometry

For $CD44^+$ subpopulation analysis, cells were suspended in 250μl ice-cold PBS and incubated with either anti-Human/Mouse CD44 PE-Cyanine5 antibody (eBioscience, catalog no. 15-0441) or Rat IgG2b K Isotype Control PE-Cyanine5 (eBioscience, catalog no. 15-4031) for 90 min at 4°C with gentle rotation. Then, the cells were washed twice with ice-cold 1×PBS before flow cytometric analysis. The data were analyzed by BD Accuri C6 Software (BD Biosciences, USA). For hoechstside-population analysis, cells were suspended in 500μl of DMEM supplemented with 10% FBS and pre-incubated with or without 100 μM verapamil (Sigma-Aldric, catalog no. V4629) for 15 min at 37°C. Subsequently, the cells were incubated with 5 μg/ml Hoechst 33342 dye (Sigma-Aldrich, catalog no. 14533) for 1 h at 37°C. Finally, the cells were incubated on ice for 5 min and washed twice with ice-cold 1×PBS before flow cytometric analysis. The data were analyzed by FlowJo 10 (FLOWJO, LLC, Ashland, USA).

Immunofluorescence and confocal microscopy assays

Spheres were collected by centrifugation at 1500×g for 5 min and gently resuspended in 1×PBS. The suspension was transferred to a glass slide and a smear was prepared. The smear was left to dry at 37°C followed by immunofluorescence analysis as described previously (Gan et al., 2016). Nuclei were stained with DAPI. Images were captured using ZEISS LSM800 confocal fluorescence microscope (ZEISS,

Germany).

Stemness signatures-related gene qPCR array

The cDNA of EC9706 cells transfected with shMTA3 or shCtrl was used for stemness signature analysis using Custom Gene qPCR Arrays (GeneCopoeia, catalog no. PAG-CS). The mRNA levels of 78 stemness genes were measured by SYBR™ Green PCR Master Mix (Applied Biosystems, catalog no. 4309155) with the Applied Biosystems 7500 Real-Time PCR system (Applied Biosystems).

Gaussia luciferase assay

Cells were transiently transfected with the indicated *Gaussia* luciferase plasmids using Lipofectamine 3000 (Thermo Fisher Scientific, catalog no. L3000015) according to the manufacturer's instructions, and incubated for 72 hours. The culture medium was collected and subjected for analysis of *Gaussia* luciferase (GLuc) and secreted Alkaline Phosphatase (SeAP) activities using a Secrete-PairTM Dual Luminescence Assay Kit (GeneCopoeia, catalog no. SPDA-D010) according to the manufacturer's instructions. GLuc activity was normalized to SeAP activity.

Chromatin immunoprecipitation assay

The chromatin immunoprecipitation (ChIP) assay was performed using an EZ-Magna ChIP™ A ChIP kit (Millipore, catalog no. 17-408) as described previously (Dong et al., 2017b). Briefly, cells were cross-linked with 1% (v/v) formaldehyde on ice for 10 minutes and sonicated to shear chromatin DNA into ~200-1000 bp in length by a Bioruptor Sonicator (Diagenode, Sparta, NJ, USA). Immunoprecipitation was done with antibodies against MTA3 (Bethyl Laboratories Inc., catalog no. A300-160A) or IgG (Sigma Aldrich, St Louis, MO, USA) with 20μl of protein A magnetic beads gently rotated at 4°C overnight. After washing by wash buffer, the immunoprecipitated DNA was then used for semi-quantitative PCR or qPCR analysis using

the following primers: P #1 forward: 5'-AGAGAATCTCAAGGTCACCAGG-3' and reverse: 5'-TGGCCATTCTTTTGCACTTGG-3'; P #2 forward: 5'-CATGCAATTACTCTGGAGGCA-3' and reverse: 5'-TTCATCACTTCTGCAATTGACCA-3'; P #3 forward: 5'-AATTGTGAACACTGTTTTTAAGCAA-3' and reverse: 5'-CCCTAAGTGTGCCATTTGCC-3'; GADPH (negative control) forward: 5'-TCCTCCTGTTTCATCCAAGC-3' and reverse: 5'-TAGTAGCCGGGCCCTACTTT-3' (Si et al., 2015). 1% of the supernatant was used as input.

Proximity ligation assay

The Proximity Ligation Assay (PLA) kit (Duolink®using PLA®Technology, Sigma–Aldrich) was employed to detect the interaction between MTA3 and GATA3 (Dong et al., 2017a). In brief, cells grown on glass coverslips were fixed with 4% paraformaldehyde followed by permeabilization in 0.2% Triton X-100 and blocking in 5% BSA. The cells were then incubated with rabbit anti-MTA3 and mouse anti-GATA3 antibodies and followed by incubation with secondary plus and minus probes, PLA–anti-(rabbit IgG) and PLA–anti-(mouse IgG). The ligation solution was added followed by an amplification solution. The PLA signals were visualized under ZEISS LSM800 confocal fluorescence microscope (ZEISS, Germany).

Animal experiments

For tumor growth assay, xenografting was performed as described previously (Dong et al., 2017b). Briefly, indicated cells (1×10^6 cells for EC9706 and EC109; 4×10^6 cells for HKESC-1) were injected subcutaneously into flanks of 5- to 6-week-old female nude mice (Vital River Laboratory Animal Technology Co. Ltd.). The tumor growth was monitored for 4 or 5 weeks. The tumor size was measured weekly using a slide caliper and tumor volume was calculated by the following formula: volume = 0.5236 $\times$ length $\times$ width^2. At the end of the experiment, mice were sacrificed and tumors were excised, photographed and used for RNA and protein purification or reserved in paraffin block. For inguinal lymph

node metastasis, cells were infected with recombinant lentiviruses carrying luciferase, and these cells (1×10^6 cells for EC9706; 5×10^6 cells for TE1) were injected subcutaneously into the flanks of 5- to 6-week-old female nude mice (8 mice per group). The mice were monitored for inguinal lymph node metastasis once weekly by injection of 150 mg/kg of D-luciferin (Solarbio, Beijing, China; catalog no. D9390) intraperitoneally. 10-15 min after injection, mice were anesthetized and bioluminescence was imaged with Xenogen IVIS System (Xenogen). Mice were sacrificed at day 32, 15 min before mice were sacrificed, D-luciferin was injected intraperitoneally. After sacrificing, the inguinal lymph nodes were harvested and analyzed for the presence of metastatic cells using Xenogen IVIS System (Xenogen). The inguinal lymph nodes were then subjected for paraffin blocks, and then tissue sections were stained with H&E for histological validation. For lung metastasis, 1×10^6 of cells were injected into the tail vein of 5- to 6-week-old female nude mice (6 mice per group). Mice were sacrificed at day 61 and the lungs were fixed in Bouins for 24 hours. The lungs were photographed, paraffin blocked, and sectioned for staining.

Bioinformatic analysis

The protein levels of MTA3 in different organs were obtained from the Human Protein Atlas database (https://www.proteinatlas.org) (Uhlen et al., 2015).ESCC datasets GSE23400 (Su et al., 2011) and GSE26886 (Wang et al., 2013) were obtained from the NCBI Gene Expression Omnibus (GEO. https://www.ncbi.nlm.nih.gov/geo/) (Barrett et al., 2007) to detect the levels of MTA3. The level of MTA3 mRNA in ESCC cell lines was analyzed in dataset GSE23964 from GEO. A TCGA dataset (Titled ESCA), which includes 81 ESCC tissues and 11 normal esophageal tissues, was downloaded from the TCGA database (https://cancergenome.nih.gov/) and analyzed. The alteration of *GATA3* gene in ESCC was analyzed using cBioPortal database (https://www.cbioportal.org/) (Gao et al., 2013).

Gene Set Enrichment Analysis

The ESCC dataset GSE23400 (Su et al., 2011) and GSE47404 (Sawada et al., 2015), head and neck squamous cell carcinoma (HNSCC) dataset GSE10300 (Cohen et al., 2009), oral squamous cell carcinoma (OSCC) dataset GSE37991 (Lee et al., 2013) from GEO, and Breast invasive carcinoma (BRCA) dataset, Pancreatic adenocarcinoma (PAAD) dataset from TCGA database were analyzed using GSEA software (Version 2.2.1, http://software.broadinstitute.org/gsea/index.jsp) as previously described (Dong et al., 2017a; Dong et al., 2017b).

Statistics

All data were analyzed using the SPSS 17.0 software (SPSS Inc., USA). Receiver operating characteristic (ROC) curve analysis was performed to define the cutoff score for the expression of MTA3 and SOX2. The $\chi2$ test was used to analyze the correlation between the expression of MTA3 and clinicopathological parameters of ESCC patients, the difference between the proportion of inguinal lymph nodes metastasis or lung metastasis in shMTA3 and shCtrl mice. Kaplan–Meier was used in plotting the survival curves, and the difference was compared by log-rank test. Univariate and multivariate Cox regression survival analyses were done to evaluate the survival data. Student's *t*-test was used to compare the difference between two groups, and one-way ANOVA with post hoc intergroup comparisons was performed to compare the difference among more than two groups. Pearson's correlation coefficients were performed to determine the correlations of the mRNA expression between *MTA3* and the indicated genes in ESCC tissues. All data were presented as the mean ± SEM. A *p*-value < 0.05 was considered statistically significant.

Study approval

Clinical research protocols of this study were reviewed and approved by the Ethics Committee of Cancer Hospital of Shantou University Medical College (IRB serial number: #04-070). Written informed consent was obtained from patients in accordance with principles expressed in the Declaration of Helsinki. Animals

were housed in conventional or pathogen-free conditions, where appropriate, at the Animal Center of Shantou University Medical College, in compliance with Institutional Animal Care and Use Committee (IACUC) regulations (SUMC2014-148). All animal experiments were performed according to protocols approved by the Animal Care and Use Committee of the Medical College of Shantou University.

Supplemental References

Barrett, T., Troup, D.B., Wilhite, S.E., Ledoux, P., Rudnev, D., Evangelista, C., Kim, I.F., Soboleva, A., Tomashevsky, M., and Edgar, R. (2007). NCBI GEO: mining tens of millions of expression profiles--database and tools update. Nucleic Acids Res *35*, D760-765.

Cohen, E.E., Zhu, H., Lingen, M.W., Martin, L.E., Kuo, W.L., Choi, E.A., Kocherginsky, M., Parker, J.S., Chung, C.H., and Rosner, M.R. (2009). A feed-forward loop involving protein kinase Calpha and microRNAs regulates tumor cell cycle. Cancer Res *69*, 65-74.

Dong, H., Ma, L., Gan, J., Lin, W., Chen, C., Yao, Z., Du, L., Zheng, L., Ke, C., Huang, X., et al. (2017a). PTPRO represses ERBB2-driven breast oncogenesis by dephosphorylation and endosomal internalization of ERBB2. Oncogene *36*, 410-422.

Dong, H., Xu, J., Li, W., Gan, J., Lin, W., Ke, J., Jiang, J., Du, L., Chen, Y., Zhong, X., et al. (2017b). Reciprocal androgen receptor/interleukin-6 crosstalk drives oesophageal carcinoma progression and contributes to patient prognosis. J Pathol *241*, 448-462.

Feng, Y., Ke, C., Tang, Q., Dong, H., Zheng, X., Lin, W., Ke, J., Huang, J., Yeung, S.C., and Zhang, H. (2014). Metformin promotes autophagy and apoptosis in esophageal squamous cell carcinoma by downregulating Stat3 signaling. Cell Death Dis *5*, e1088.

Gan, J., Ke, X., Jiang, J., Dong, H., Yao, Z., Lin, Y., Lin, W., Wu, X., Yan, S., Zhuang, Y., et al. (2016). Growth hormone-releasing hormone receptor antagonists inhibit human gastric cancer through downregulation of PAK1-STAT3/NF-kappaB signaling. Proc Natl Acad Sci U S A *113*, 14745-14750.

Gao, J., Aksoy, B.A., Dogrusoz, U., Dresdner, G., Gross, B., Sumer, S.O., Sun, Y., Jacobsen, A., Sinha, R., Larsson, E., et al. (2013). Integrative analysis of complex cancer genomics and clinical profiles using the cBioPortal. Sci Signal *6*, pl1.

Lee, C.H., Wong, T.S., Chan, J.Y., Lu, S.C., Lin, P., Cheng, A.J., Chen, Y.J., Chang, J.S., Hsiao, S.H., Leu, Y.W., et al. (2013). Epigenetic regulation of the X-linked tumour suppressors BEX1 and LDOC1 in oral squamous cell carcinoma. J Pathol *230*, 298-309.

Sawada, G., Niida, A., Hirata, H., Komatsu, H., Uchi, R., Shimamura, T., Takahashi, Y., Kurashige, J., Matsumura, T., Ueo, H., et al. (2015). An Integrative Analysis to Identify Driver Genes in Esophageal Squamous Cell Carcinoma. PLoS One *10*, e0139808.

Si, W., Huang, W., Zheng, Y., Yang, Y., Liu, X., Shan, L., Zhou, X., Wang, Y., Su, D., Gao, J., et al. (2015). Dysfunction of the Reciprocal Feedback Loop between GATA3- and ZEB2-Nucleated Repression Programs Contributes to Breast Cancer Metastasis. Cancer Cell *27*, 822-836.

Su, H., Hu, N., Yang, H.H., Wang, C., Takikita, M., Wang, Q.H., Giffen, C., Clifford, R., Hewitt, S.M., Shou, J.Z., et al. (2011). Global gene expression profiling and validation in esophageal squamous cell carcinoma and its association with clinical phenotypes. Clin Cancer Res *17*, 2955-2966.

Uhlen, M., Fagerberg, L., Hallstrom, B.M., Lindskog, C., Oksvold, P., Mardinoglu, A., Sivertsson, A., Kampf, C., Sjostedt, E., Asplund, A., et al. (2015). Proteomics. Tissue-based map of the human proteome. Science *347*, 1260419.

Wang, Q., Ma, C., and Kemmner, W. (2013). Wdr66 is a novel marker for risk stratification and involved in epithelial-mesenchymal transition of esophageal squamous cell carcinoma. BMC Cancer *13*, 137.